Ammonia-salt solvent promotes cellulosic biomass deconstruction under ambient pretreatment conditions to enable rapid soluble sugar production at ultra-low enzyme loadings

Shishir P. S. Chundawat,[a]* Leonardo da Costa Sousa,[b] Shyamal Roy,[a,c] Zhi Yang,[d] Shashwat Gupta,[a] Ramendra Pal,[e] Chao Zhao,[a,f] Shih-Hsien Liu,[g] Loukas Petridis,[g] Hugh O'Neill,[d] Sai Venkatesh Pingali[d]

Here, we report a novel ammonia:ammonium salt solvent based pretreatment process that can rapidly dissolve crystalline cellulose into solution and eventually produce highly amorphous cellulose under near-ambient conditions. Pre-activating the cellulose I allomorph to its ammonia-cellulose swollen complex (or cellulose III allomorph) at ambient temperatures facilitated rapid dissolution of the pre-activated cellulose in the ammonia-salt solvent (i.e., ammonium thiocyanate salt dissolved in liquid ammonia) at ambient pressures. For the first time in reported literature, we used time-resolved *in-situ* neutron scattering methods to characterize the cellulose polymorphs structural modification and understand the mechanism of crystalline cellulose dissolution into a 'molecular' solution in real-time using ammonia-salt solvents. We also used molecular dynamics simulations to provide insight into solvent interactions that non-covalently disrupted the cellulose hydrogen-bonding network and understand how such solvents are able to rapidly and fully dissolve pre-activated cellulose III. Importantly, the regenerated amorphous cellulose recovered after pretreatment was shown to require nearly ~50-fold lesser cellulolytic enzyme usage compared to native crystalline cellulose I allomorph for achieving near-complete hydrolytic conversion into soluble sugars. Lastly, we provide proof-of-concept results to further showcase how such ammonia-salt solvents can pretreat and fractionate lignocellulosic biomass like corn stover under ambient processing conditions, while selectively co-extracting ~80-85% of total lignin, to produce a highly digestible polysaccharide-enriched feedstock for biorefinery applications. Unlike conventional ammonia-based pretreatment processes (e.g., Ammonia Fiber Expansion or Extractive Ammonia pretreatments), the proposed ammonia-salt process can operate at near-ambient conditions to greatly reduce the pressure/temperature severity necessary for conducting effective ammonia-based pretreatments on lignocellulose.

Introduction

Native cellulose derived from lignocellulosic biomass is a β-1,4-D-glucose polymer with extensive intra- and inter-molecular hydrogen bonding that stabilizes its ordered crystalline structure and makes it highly recalcitrant to cellulase enzyme-catalyzed degradation into soluble sugars.[1–3] Disruption of cellulose crystallinity using suitable solvents or thermochemical pretreatments is thus necessary to make polysaccharides more readily accessible to cellulolytic enzymes[4,5] or suitable chemicals/catalysts[6,7] that facilitate cellulose hydrolysis to glucose. One major advantage of pretreatment solvents that can significantly disrupt cellulose crystallinity, while possibly selectively co-extracting lignin, is the significant reduction in enzyme usage that could make cellulosic biorefineries economically more viable.[8] Most enzyme loadings reported currently for saccharification of crystalline cellulose or pretreated biomass is still at least an order of magnitude (10-15 mg enzymes/g cellulose) higher than what is likely to be commercially viable,[9] similar to advanced corn grain dry-grind processes that often use <0.5-1 mg enzyme/g starch loading.[10] Therefore, there is a critical need to identify pretreatments that can significantly disrupt cellulose crystallinity to reduce enzyme loadings during biomass saccharification by at-least 10-fold from current usage.

Over the last 150 years several non-derivatizing solvents, like ionic liquids (IL), have been employed to readily dissolve cellulose and/or disrupt cellulose crystallinity to produce highly disordered or regenerated amorphous cellulose.[11,12] Disordered or regenerated amorphous cellulose (RAC) recovered after disruption of native cellulose crystallinity has been shown to

[a] *Department of Chemical & Biochemical Engineering, Rutgers The State University of New Jersey, Piscataway, NJ 08854, USA*. *Corresponding Author Email: shishir.chundawat@rutgers.edu
Department of Chemical Engineering & Materials Science, Michigan State University, East Lansing, MI 48824, USA.
Department of Chemical Engineering, Jadavpur University, Jadavpur, Kolkata, West Bengal 700032, India. (Current Address)
Center for Structural Molecular Biology, Oak Ridge National Laboratory, Oak Ridge, TN 37831, USA.
Department of Mechanical & Aerospace Engineering, Rutgers The State University of New Jersey, Piscataway, NJ 08854, USA.
School of Engineering, Zhejiang A&F University, Linan, Zhejiang 311300, People's Republic of China. (Current Address)
UT/ORNL Center for Molecular Biophysics, Oak Ridge National Laboratory, Oak Ridge, Tennessee 37831, USA.

result in significantly enhanced enzymatic hydrolysis rates.[13,14] However, most reported cellulose solvents are fairly expensive and difficult to recycle.[5,14,15] For example, most commercially available imidazolium based IL cost >$50/kg,[12] but there have been advances in recent years to develop lower cost IL and pretreatment-solvent recycle strategies to reduce effective IL cost to ~$5/kg.[5,16] Nevertheless, alternative inexpensive solvent systems with cellulose dissolution properties similar to conventional IL are still being explored.

Several research groups have studied the impact of ammonia pretreatment on cellulose crystallinity and its beneficial impact on cellulolytic enzyme activity.[3,17–20] Anhydrous liquid ammonia (NH_3) acts as a swelling agent of cellulose by intercalating into the crystalline structure of cellulose and disrupting the native hydrogen bonding network to form a metastable cellulose-ammonia complex.[19,21–23] An unnatural crystalline cellulose allomorph, called cellulose III, is formed from these swollen cellulose-ammonia complexes upon immediate removal of ammonia. We have shown that selective '*rewiring*' of the cellulose hydrogen bond network within cellulose III can enhance synergistic enzymatic hydrolysis rates by several fold, but hydrolysis rates for crystalline cellulose was still much lower than RAC.[3] Subsequently, a novel liquid ammonia pretreatment methodology called Extractive Ammonia (EA) was developed to simultaneously convert native crystalline cellulose I into cellulose III allomorph, while also partially extracting lignin from lignocellulosic biomass like corn stover, to improve upon the traditional Ammonia Fiber Expansion (AFEX) process.[24] However, although ammonia is inexpensive (<$0.5/kg) and readily recoverable due to its high volatility,[25,26] effective biomass pretreatments with ammonia alone during EA or AFEX pretreatments require high severity operating pressures (250-1500 psi) and temperatures (90-130 °C). Furthermore, although crystalline cellulose III has improved enzymatic digestibility compared to native cellulose I, it is still more recalcitrant towards hydrolysis than truly amorphous cellulose (or RAC) produced in IL-based pretreatments.

One strategy to reduce ammonia-based pretreatment severity to ambient conditions while fully disrupting cellulose crystallinity would be to add a co-solvent/chemical that can reduce NH_3 partial pressure while also facilitating rapid cellulose dissolution. We have recently shown that co-solvents like ethanol can reduce the operating pressure during EA pretreatment by ~2-fold without hindering the formation of the cellulose-ammonia complex that leads to cellulose III.[27] However, inclusion of ammonium salts can reduce the vapor pressure of NH_3 by nearly 30-fold (at 25 °C),[28] which can greatly reduce the thermochemical severity of a theoretical ammonia-salt treatment process compared to conventional NH_3 based treatments.[28,29] Furthermore, inclusion of hydrogen-bond acceptor anion (e.g., SCN^- or I^-) based ammonium salts with NH_3 has been reported to remarkably facilitate complete dissolution of regenerated cellulose.[30,31] However, native crystalline cellulose I dissolution in an ammonia-ammonium thiocyanate (NH_3-NH_4SCN) or A:At based ammonia-salt solvent can only take place by extensive thermal cycling of the cellulose-solvent slurry by first exposure to extreme freezing temperatures (-80 to -30 °C) followed by mechanical stirring of the slurry as the temperature is slowly raised to room temperature over 6-12 hours, followed again by multiple freeze-thaw cycles of the slurry till the cellulose is fully dissolved into solution.[32,33] In the absence of multiple freeze-thaw thermal cycles, native crystalline cellulose can take several days at room temperature to be only partially dissolved in NH_3-NH_4SCN. Such an extreme temperature cycling requirement to achieve complete cellulose dissolution over several days makes this originally reported process not ideal for cellulosic biomass pretreatment in a biorefinery setting. *Furthermore, we currently still have a poor understanding of the in-situ mechanism of real-time cellulose dissolution in ammonia-salt solvents which has further led to limited advances to original process reported by Cuculo.*[31]

One strategy to design a more efficient ammonia-salt pretreatment process would be to take advantage of recent advances in our understanding of ammonia-cellulose interactions during liquid NH_3 based pretreatments. Our recent experimental[3,27] and modeling[34–36] studies have revealed the early mechanism of crystalline cellulose swelling that takes place nearly instantaneously in the presence of liquid NH_3, which ultimately results in the formation of cellulose III only upon removal of NH_3. Molecular dynamics (MD) simulations of ammonia-cellulose interactions suggested NH_3 first hydrogen bonds with cellulose fibril surface exposed hydroxyl groups, which results in the rotation of the C6-hydroxymethyl groups from Trans-Gauche (TG) to Gauche-Trans (GT) conformations. This GT conformation change instantly leads to the formation of hydrophilic channels in the crystalline fibril to form an intermediate structure that resembles the cellulose-ammonia complex.[34,36] Crystallographic evidence has also verified the formation of these channels that allow bulk NH_3 molecules to penetrate into the fibril and cause further swelling of individual cellulose crystalline fibers.[37] However, unlike true cellulose dissolving solvent systems like imidazolium acetate IL where both anionic and cationic solvent species are necessary to dissolve individual cellulose polymer chains,[38] NH_3 alone is unable to fully disrupt the internal cellulose crystal hydrogen bonding network to solubilize individual cellulose chains. *We hypothesized that first pre-activation of native crystalline cellulose to its ammonia-cellulose swollen complex at ambient temperatures would allow improved accessibility of the ammonia-salt ions through the hydrophilic channels into the core fibril.* Addition of the anionic salts like ammonium thiocyanate immediately after pre-swelling the cellulose in ammonia could allow rapid dissolution of the pre-activated cellulose under ambient pressures and temperatures. No one has so far studied the effect of pre-activation of cellulose on its dissolution kinetics in NH_3-NH_4SCN solvent, or studied the multi-length scale cellulose dissolution dynamics using suitable scattering techniques, or developed an ammonia-salt based pretreatment for biochemical conversion of biomass into soluble sugars.

Here, we have tested the cellulose pre-activation hypothesis to explore the possibility of developing an ammonia-salt solvent-based pretreatment method that operates under ambient conditions to rapidly and completely solubilize cellulose. We have used *in-situ* neutron scattering to follow the real-time dissolution of cellulose in the ammonia-salt solvent, and provide fundamental insights into the pretreatment mechanism. Molecular dynamics simulations were also used to support our hypothesis and to fully understand the mechanism of model cellulose polymers dissolution in A:At based solvent systems. We also conducted detailed enzymatic saccharification assays at varying enzyme loadings for the cellulose recovered after treatment with the ammonia-salt solvent to compare the impact of pretreatment on cellulase activity. Finally, we provide proof-of-concept results showing how ammonia-salt solvents can effectively pretreat and selectively fractionate complex lignocellulosic biomass like corn stover into its constituent biopolymers under ambient pretreatment conditions.

Materials and Methods

Microcrystalline Cellulose & Biomass Feedstocks

High purity (>98% cellulose content, dry weight mass basis or dwb) microcrystalline cellulose, purchased from Sigma-Aldrich (Avicel PH-101, Lot No. BCBD6923V), was used here. This original sample, called Avicel cellulose I or CI, also served as the native cellulose I allomorph standard. Pre-activated crystalline cellulose III (or CIII) was produced from CI using anhydrous liquid ammonia as reported previously.[3,27] Briefly, CIII was prepared in a high-pressure stirred batch reactor at desired temperature (e.g., 25 or 90 °C) for 30 min residence time using a 6:1 ammonia-to-cellulose loading ratio (on dry cellulose weight basis or dwb). The reactor pressure was maintained constant using nitrogen gas during pretreatment, and ammonia was slowly evaporated from the reactor through a venting valve after 30 min. During this evaporation process, the temperature of the reactor was kept stabilized at 25 °C. The treated cellulose sample was then removed from the reactor and placed overnight in the fume hood to evaporate any residual ammonia. No additional washing steps were employed other than using nitrogen gas and overnight fume hood drying to remove all traces of ammonia from the treated cellulose samples. All treated cellulose samples were stored at 4 °C in a zip sealed bag prior to usage. The CIII sample had a total moisture content less than 6-7% (on total wet cellulose weight basis or twb) and was used directly for all further ammonia-salt pretreatment studies without any further drying. Lastly, pioneer 36H56 corn hybrid derived corn stover was generously provided by the Great Lakes Bioenergy Research Center and processed for handling as described earlier.[24] Details regarding corn stover composition analysis method and results is provided in the ESI appendix.

Ammonia-Ammonium Thiocyanate Salt Based Pretreatments

Unless noted otherwise, commercial grade anhydrous ammonia (>99.99% NH_3 purity from Airgas, Lawrenceville, GA) and ammonium thiocyanate (>99% NH_4SCN purity from Sigma-Aldrich, St. Louis, MO) were used here as is without any drying for all *ex-situ* pretreatment studies. Deuterated ammonia-d_3 (99% atom isotopic purity ND_3, Sigma-Aldrich, St. Louis, MO), deuterated ammonium-d_4 thiocyanate (99% atom isotopic purity ND_4SCN, Sigma-Aldrich, St. Louis, MO), and deuterated water-d_2 (99.9% atom isotopic purity D_2O, Sigma-Aldrich, St. Louis, MO) were used for all *in-situ* neutron scattering pretreatment studies. Analytical grade Acetone and 200 Proof Ethanol solvents were procured from Sigma-Aldrich and VWR Scientific, respectively.

To prepare the ammonia-salt solution for cellulose pretreatment, the required dry weight of ammonium salt was transferred into a high-pressure sealed vessel (Parr) followed by slowly loading ammonia into the vessel while weighing the reactor intermittently to achieve targeted ammonia loading. After a stable ammonia-salt solution is formed, transfer the solution into an amber stained Schott glass bottle with screw cap for storage under ambient conditions in fume hood. This colourless solution was stable at room temperature for several months and was used directly for biomass pretreatment.

Native (CI) or pre-activated microcrystalline (CIII) cellulose was pretreated using a 27:73% (weight basis; w/w) ammonia-ammonium thiocyanate solution as described below. This solvent concentration has been reported previously to be ideal for cellulose dissolution.[31,39] For all *ex-situ* ammonia-salt pretreatments, 5 g of either cellulose I or cellulose III (on twb) was added along with 95 g of ammonia-salt solution (i.e., 95 g of solution was composed of 69.4 g ammonium thiocyanate salt dissolved in 25.6 g ammonia) in a 500 mL stoppered glass bottle. The slurry was mixed using a magnetic stirrer at 500 rpm for desired pretreatment time (0.5-72 h) at ambient pressure and temperature. At the desired sampling time, 100 mL of ethanol (100%) was added as anti-solvent to precipitate cellulose out of solution. The precipitate was washed with excess ethanol (50:1, v/w), followed by five washes with 1:1 ethanol-acetone (20:1, v/w) to remove any trace residual ammonia-salt. Treated cellulose samples were stored in a never-dried state, soaked in 100% ethanol, at 4 °C prior to usage. Details regarding corn stover pretreatment and additional cellulose ultrastructure characterization using X-Ray Diffraction (XRD) and Scanning Electron Microscopy (SEM) based methods is provided in the ESI appendix (**ESI M1-M4**).

Small Angle Neutron Scattering (SANS)

SANS measurements were performed with the CG-3 Bio-SANS instrument at the High Flux Isotope Reactor (HFIR) facility of Oak Ridge National Laboratory.[40] Samples for SANS studies were placed in either a 1 mm thick Hellma cell (Hellma Model #106-QS 1MM) or 1.0 mm thick titanium cells with detachable cell walls. The choice of the cell was based on sample state; viscous samples were placed in titanium cells with detachable cell walls to allow for eliminating bubbles from the illuminated region of the sample. A single instrument configuration was employed to cover the range, $0.003<Q(\text{Å}^{-1})<0.8$, of scattering vectors. The scattering vector Q is related to λ, neutron wavelength and 2θ, the scattering angle as $Q = 4\pi \sin\theta/\lambda$.

Using 6 Å neutron wavelength, main detector at 15.5 m from sample and wing detector at 1.4° rotation from direct beam, a sufficient overlap in scattering vectors to stitch data from the two detectors was achieved. The instrument resolution was defined placing source and sample circular apertures at 17430 mm apart and with diameters 40 mm and 14 mm, respectively. The relative wavelength spread $\Delta\lambda/\lambda$ was set to 0.15. The scattering intensity profiles $I(Q)$ versus Q, were obtained by azimuthally averaging the processed 2D images, which were normalized to incident beam monitor counts, and corrected for detector dark current, pixel sensitivity and scattering from the quartz cell walls and solvent scattering backgrounds. SANS data was analyzed using the multilevel unified equation implemented in Irena Package to elucidate the multiple levels of structural organization.[41] Irena is an Igor Pro software package consisting of various structural models to analyze small-angle scattering data. For each individual level, i, the scattering signal is the sum of Guinier's exponential form and the structurally limited power-law as,[42–44]

$$I(Q) = \sum_{n=1}^{\infty} [G_i \exp\left(-\frac{Q^2 R_{g_i}^2}{3}\right) + B_i \exp\left(-\frac{Q^2 R_{g_{(i-1)}}^2}{3}\right) \{\left[\mathrm{erf}\left(\frac{Q R_{g_i}}{\sqrt{6}}\right)\right]^3 / Q\}^{P_i}] + I_{bkg}$$

where $i = 1, \ldots, n$. To model the cellulose SANS data, we used a total of three levels with $i = 1$ and $i = 3$ referring to the smallest and largest size structural levels, respectively. Here, $G_i = c_i V_i \Delta\rho_i^2$ is the exponential prefactor, where c_i is the concentration of the i^{th} kind of particle; V_i is the volume of the particle and $\Delta\rho_i$ is the contrast of the i^{th} kind of particle with respect to the solvent; R_{g_i} is the radius of gyration describing the average size of the i^{th} level structural unit; B_i is a Q-independent prefactor specific to the type of power-law scattering with power-law exponent P_i and I_{bkg} is the flat background intensity due to incoherent scattering.[42]

Ex-situ neutron scattering experiments were performed on regenerated cellulose recovered directly after ammonia-salt treatment of cellulose samples for varying conditions. For SANS experiments, the cellulose samples were centrifuged and then resuspended in 100 % D_2O solvent at a 1:10 ratio to exchange the labile hydroxyl hydrogens in cellulose prior to SANS characterization of cellulose samples suspended in 100 % D_2O solvent. This exchange process was repeated three times. The final concentration of all *ex-situ* pretreated and D_2O solvent exchanged cellulose was 50 g/L. *In-situ* neutron scattering experiments were performed on native cellulose I or pre-activated cellulose III in real-time to study cellulose dissolution dynamics in deuterated and protiated ammonia-salt solvent at room temperature/pressure for varying dissolution time periods (0.5-72 h). The concentration of all *in-situ* cellulose samples suspended in the ammonia-salt solvent was ~2% (w/v). The deuterated or protiated ammonia-salt solutions composition was identical to the *ex-situ* experiments (i.e., 95 g of 27:73% w/w ammonia-salt solution was composed of 69.4 g ammonium thiocyanate salt dissolved in 25.6 g ammonia).

Cellulosic Biomass Enzymatic Hydrolysis

All pretreated cellulose samples were subjected to enzymatic hydrolysis using a commercial cellulase cocktail at 0.4% glucan loading in a 0.2 ml reaction volume using microplates based on the original high-throughput assay,[45] with some minor modifications as described below. Assays for varying cellulase loading and saccharification time course were conducted in 200 µL total volume (using 0.5 ml Greiner microplates sealed with Micronic TPE capclusters) that comprised of 80 µL of 10 g/L cellulosic substrate slurry added along with 100 µL of 50 mM pH 4.8 sodium acetate buffer, and 20 µL of suitably diluted enzyme stock to desired protein loadings (i.e., mg total enzyme loading per gram of added cellulose per well). Stock cellulosic substrate slurry was prepared in deionized water with sodium azide (0.2% w/v) added to prevent microbial growth. The total protein loadings used during enzymatic hydrolysis ranged between 0.025 to 5 mg enzyme/g glucan of Cellic C.Tec2 enzymes (Novozymes, CA). The protein concentration (40 mg/ml) for the enzyme stock solutions was determined using the Bradford method.[46] The microplates were incubated at 50 °C with 5 rpm end-over-end mixing oven for desired saccharification time (0-120 h). All pretreated corn stover samples were subjected to enzymatic hydrolysis at 2.5% glucan loading in 10 ml reaction volume using 15 ml glass vials as described before,[3] based on the original NREL protocols.[47] In all assays, final reaction volume pH 4.8 was achieved using 50 mM sodium citrate buffer and sodium azide was added to prevent any microbial growth (0.1% w/v final concentration). Vials were incubated at 50 °C in an orbital shaking incubator set at 150 RPM (New Brunswick, Innova 44, Enfield, CT) for the desired saccharification time.

The hydrolysate supernatants were analyzed for total reducing sugar concentrations using the standard dinitrosalicylic acid (DNS) colorimetric assay or glucose/xylose based enzymatic assay kits as reported earlier.[48] Briefly, 30 µl of the cellulose hydrolysate supernatant was incubated with 60 µl of DNS stock reagent in PCR plates at 95 °C for 5 min in an Eppendorf thermal cycler. After the PCR plates cooled down to room temperature, transfer and dilute the DNS reaction mixture in DI water using a clear, flat-bottom microplate for measuring solution absorbance at 540 nm. Suitable reducing sugar standards (e.g., glucose standards ranging from 0.1–5 g/l) were included for the DNS assay. Glucose concentrations in corn stover hydrolyzates was determined using suitable enzymatic assay kit from Megazyme (Bray, Ireland).[48] All hydrolysis experiments were carried out in at least triplicates with typically less than ±10% standard deviation from reported mean values. Glucan conversion to glucose was quantified as described in the NREL protocol.[47] Specific activity of the cellulase cocktail on various cellulose substrates was determined from the varying ultra-low enzyme loading assay dataset after 24 h incubation period.[46] One unit of specific cellulase activity was defined as 1 µmol reducing sugars (as glucose equivalents) released per milligram enzyme per minute. Error bars reported in this work

represent one standard deviation (±1σ) from mean values for replicate assays.

Molecular Dynamics (MD) Simulations of Cellulose-A:At Solvent

MD simulation methods (**ESI M5 & Tables S2-S4**) and detailed supporting results are provided in the ESI appendix.

Results and Discussion

Pre-activation of cellulose facilitates rapid solvent dissolution

We tested our cellulose pre-activation hypothesis by dissolving two distinct crystalline allomorphs of cellulose using an A:At solvent at room temperature for varying durations ranging from 1-24 h (**Figure 1A**). To our surprise, pre-activated cellulose III started to dissolve nearly instantly upon contact with the A:At solvent (**Figure 1B**), unlike native cellulose I which took over several hours to show any visible change in the cellulose slurry transparency/viscosity. In order to characterize the degree of decrystallization as a function of pretreatment duration, cellulose regenerated from the A:At solution using ethanol as anti-solvent was lyophilized and characterized by XRD and SEM. XRD clearly shows a significant drop in the equatorial crystallite peak reflections for (101), $(10\bar{1})$, and (002) crystallographic planes for cellulose III within 1 h of A:At treatment with close to baseline signals (**Figure 1D**). SEM analysis also confirmed that lyophilized A:At treated cellulose III had completely lost all fibril like features seen in native microcrystalline cellulose (**ESI Figure S1**). However, cellulose I shows a rather slow, but progressive, decrease in the equatorial reflections as a function of A:At treatment time (**Figure 1C**). Even after 24 h cellulose I was only partial dissolved in A:At as indicated by the relatively strong XRD equatorial reflections for the (002) crystallographic plane in particular for recovered and regenerated samples. Details regarding analysis of cellulose crystallinity index for all lyophilized samples using XRD peak deconvolution method is provided in the ESI appendix (**ESI Figure S2 & Table S1**).

Ammonia-salt treated cellulose is easily hydrolyzed by cellulases

Next, we systematically characterized the hydrolysis activity of a commercial cellulase enzyme cocktail (Cellic C.Tec2 from Novozymes) at varying total enzyme loadings and durations of saccharification time for all A:At treated cellulose samples (**Figure 2**). Firstly, we found that all A:At treated cellulose samples always resulted in a pretreated substrate that was significantly less recalcitrant towards cellulase activity. The degree of cellulose crystallinity disruption, quantified as recovered lyophilized cellulose crystallite size, was seen to be

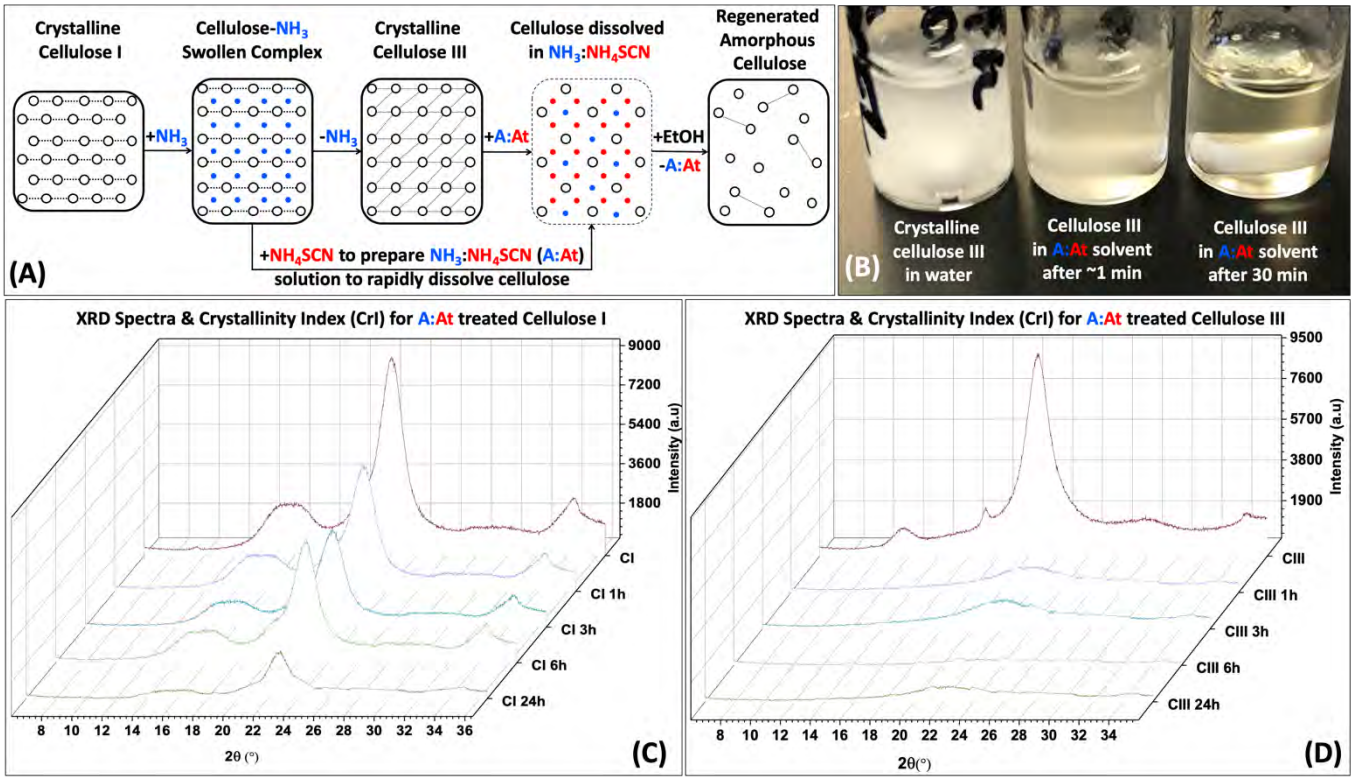

Figure 1. **Pre-activation of crystalline cellulose with ammonia facilitates rapid dissolution in ammonia:ammonium thiocyanate (A:At) based ammonia-salt solvent system.** (A) Schematic outlining cross-sectional view of model cellulose I fibril and how it can be pre-activated to a swollen cellulose-ammonia complex, or ultimately cellulose III allomorph, to facilitate salt penetration into crystalline matrix to fully solubilize individual cellulose chains into an A:At solution. The dissolved cellulose can be then regenerated as highly amorphous cellulose using a suitable antisolvent like ethanol. The dotted lines represent inter-molecular hydrogen-bonding between cellulose chains. (B) Picture showing how A:At solution can nearly instantly solubilize cellulose III within a few minutes of contact to give rise to a clear solution. X-ray diffraction (XRD) was carried out on lyophilized amorphous cellulose regenerated from A:At solution treated cellulose I (C) and cellulose III (D) for increasing durations of treatment time (1-24 h) at room temperature and pressure. XRD spectra reveals pre-activated cellulose III is nearly completely decrystallized within a few hours of A:At treatment while cellulose I is still mostly crystalline and intact even after 24 hours. Here, control cellulose I and cellulose III XRD spectra are shown in dark magenta; while 1, 3, 6, and 24 hours treated samples are shown in purple, cyan, green, and olive brown, respectively. Cellulose crystallite sizes for all A:At treated cellulose samples, based on the XRD peak deconvolution method, is outlined in the ESI section.

inversely correlated to the enzymatic hydrolysis yield of the never-dried recovered cellulose samples (**Figure 2A**). It should be noted that lyophilization of amorphous cellulose from wet slurries can cause significant cellulose recrystallization and lower cellulase accessibility. This makes it challenging to draw clear correlations between XRD for dried samples versus enzymatic hydrolysis data for never-dried samples.[49] We have also conducted enzymatic hydrolysis on all lyophilized samples to show a clear drop in overall hydrolysis yields (**ESI Figure S3**). Nevertheless, here again we see that A:At treated cellulose III was significantly more digestible than cellulose I or III controls.

Furthermore, we studied the effect of total cellulase loading (i.e., mg enzyme/g cellulose) for all never-dried A:At pretreated cellulose samples. Representative 24 h saccharification results for cellulose allomorph controls and their respective 6 h A:At treated samples are shown here (**Figure 2B and 2C**). These results clearly demonstrate that A:At treated cellulose III required much lower enzyme loadings to achieve near-theoretical conversion. Relative initial specific activity of the cellulase cocktail was determined to be close to an order of magnitude higher for A:At treated cellulose III versus native cellulose I (~9.1 vs. 1 μmol glucose released per mg enzyme per min, respectively). Specific cellulase activity on control amorphous cellulose (i.e., PASC) under identical assay conditions was ~6.5 μmol/mg/min. Interestingly, relative specific activity of the cellulase cocktail was comparable for A:At treated cellulose I and cellulose III (~1.4 μmol glucose released per mg enzyme per min). Similar enzyme loading effects on cellulose conversion trends were seen for other pretreatment conditions as well, therefore, detailed data is not reported here. See ESI for representative saccharification data reported for other A:At pretreated samples.

However, since neither native cellulose I or cellulose III gave maximum theoretical yields after 24 h, we also conducted kinetic time course saccharification assays over 5-days to determine the maximum conversion possible at ultra-low (i.e., 0.1, 0.5 mg/g glucan loading) and low (i.e., 5 mg/g glucan loading) enzyme loadings. The saccharification time course

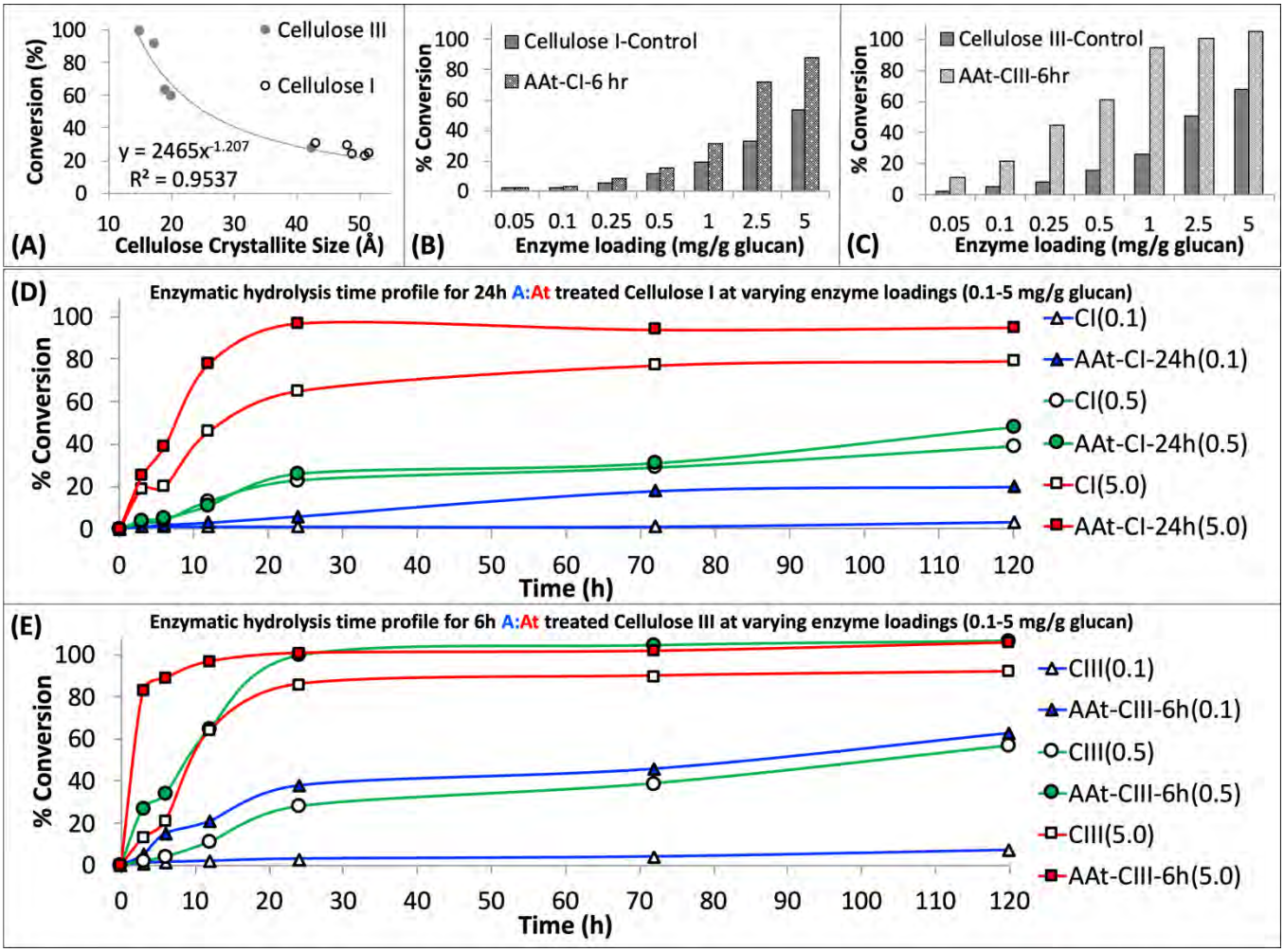

Figure 2. **Regenerated amorphous cellulose recovered after ammonia:ammonium thiocyanate (A:At) pretreatment of crystalline cellulose can be readily hydrolyzed by cellulases.** (A) A:At solvent pretreatment of cellulose results in reduction of cellulose crystallite size, estimated by deconvoluted XRD peaks analysis by Scherrer method for all cellulose I and cellulose III samples treated for varying durations. The crystallite size was inversely proportional to the cellulase catalyzed cellulose-to-glucose saccharification yield. See ESI appendix for details on crystallite size analysis details. Cellulase enzyme dosage response studies revealed that A:At treated pre-activated cellulose III (C) gives higher hydrolysis yields versus both native and A:At pretreated cellulose I (C) after 24 hours of saccharification. Here, cellulose I and cellulose III were both treated by A:At for 6 h for sake of comparison. Lastly, detailed cellulase hydrolysis kinetics time course profile over 0-120 h is shown for native/A:At treated cellulose I (D) and cellulose III (E) at three different cellulase enzyme loadings (i.e., 0.1, 0.5, and 5 mg enzyme/g glucan). Here, 24 h A:At treated cellulose I and 6 h A:At treated cellulose III were compared for their relative hydrolysis time profiles.

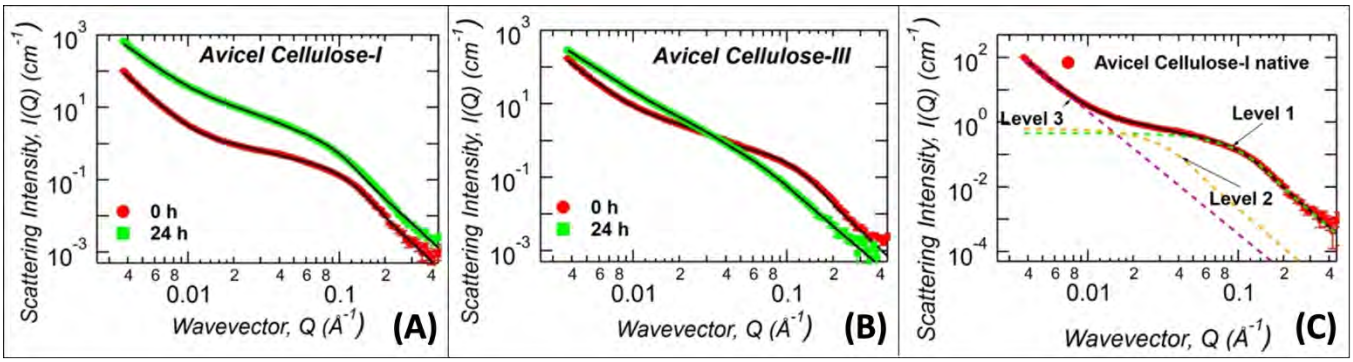

Figure 3. **Ex-situ ammonia:ammonium thiocyanate (A:At) pretreatment derived regenerated amorphous cellulose (RAC) were characterized by Small Angle Neutron Scattering (SANS).** (A) Protiated A:At pretreated cellulose I (for 24 hours treatment time at room temperature/pressure prior to recovery of RAC) SANS scattering profile is shown here in green squares, while control untreated cellulose I (0 h) is shown in red dots. (B) Protiated A:At pretreated cellulose III (for 24 hours treatment time at room temperature/pressure prior to recovery of RAC) SANS scattering profile is shown here in green squares, while control cellulose III (0 h) is shown in red dots. (C) A representative unified model fit curve is shown as a solid black line fitted to cellulose I data (in red), along with individual levels shown as green (level 1), gold (level 2), magenta (level 3) dashed lines. The solid black lines in (A) and (B) are the unified fits to the experimental SANS data with results shown in Table 1. Note that all samples were exchanged in to D_2O solvent prior to analysis and were never dried.

assay revealed that both cellulose allomorphs never achieved complete hydrolysis even at the highest 5 mg/g loading after 5 days (**Figure 2D**). This is not surprising since slow but steady deactivation of cellulase enzymes at the air-liquid interface has been shown to be main factor responsible for incomplete cellulose digestion at low enzyme loadings of 5 mg/g glucan.[50] However, A:At pretreated cellulose samples were able to achieve near-theoretical conversion even at the 0.5 mg/g glucan loading within 24 h (**Figure 2E**). Improved substrate accessibility and reduced recalcitrance of the A:At pretreated cellulose III sample to hydrolytic cellulases is clearly beneficial to achieve rapid saccharification at ultra-low enzyme loadings that overcomes the challenges of enzyme deactivation during prolonged multi-day durations. Even with a much lower enzyme loading of 0.1 mg/g glucan, A:At pretreated cellulose III was able to digest nearly 2/3^{rds} of the substrate within 5 days while native cellulose I and control cellulose III allomorphs both showed only 5-7% conversion after 5 days. In fact, close to 2/3^{rds} hydrolysis of native cellulose I was only seen at ~50-fold higher enzyme loading unlike A:At pretreated cellulose III.

SANS analysis of never-dried A:At treated cellulose ultra-structure

The never-dried cellulose recovered after A:At pretreatment could not be used to glean detailed structural information using XRD, and therefore SANS was used to characterize the never-dried cellulose samples (**Figure 3, ESI Figure S4**). Here, all samples were *ex-situ* pretreated using protiated A:At solvent for 24 h and the regenerated amorphous cellulose recovered was directly analyzed without lyophilization, after exchange into D_2O. All Avicel based cellulose samples were analyzed with three structural levels of the Unified Fit model: high-*Q* (> 0.06 Å^{-1}), mid-*Q* (0.008 < *Q* < 0.06 Å^{-1}), and low-*Q* regions (< 0.008 Å^{-1}), as illustrated in **Figure 3C** and the model fit values of the structural parameters are listed in **Table 1**.

High-*Q* R_g represents the crystalline cellulose microfibril cross-sectional dimension,[44,51] while the mid-*Q* R_g represents the size of the cellulose microfibril bundles or aggregates which are not necessarily crystalline in arrangement. Note that, R_g, is a shape independent parameter and should be multiplied by a factor of 2.3 to convert the high-*Q* R_g and mid-*Q* R_g values to true cellulose microfibril and bundle cross-sectional diameter, respectively. Both the cellulose microfibril size (high-*Q* R_g) and the cellulose bundle size (mid-*Q* R_g) show marginal change upon treatment of cellulose I with A:At (**Figure 3A**). This indicates minimal penetration and disruption of A:At into the crystalline core of cellulose even after extensive 24 hours of dissolution time. However, in the low-*Q* region, which is sensitive to length scales up to 200 nm, the SANS profile follows a power-law decay. A power-law exponent of 4 represents a smooth surface while 3 represents a highly rough surface. The power-law exponent decreased from 4.0 ± 0.1 to 3.0 ± 0.1 after A:At treatment of cellulose I indicating that the surface morphology of the larger aggregates became rough upon treatment. This implies that A:At only disrupts larger aggregates of cellulose-I by slowly disrupting its surfaces while smaller crystalline core structures are still largely intact.

In contrast, the high-*Q* cellulose microfibril size feature disappeared completely after A:At pretreatment of ammonia

Sample Type	High-*Q* R_g (Å)	High-*Q* exponent, *P*	Mid-*Q* R_g (Å)	Mid-*Q* exponent, *P*	Low-*Q* exponent, *P*
CI control	20 ± 1	4 #	60 ± 10	4 #	4.0 ± 0.1
AAt-CI 24h-treated	23 ± 2	4 #	64 ± 6	4 #	3.0 ± 0.1
CIII control	18.6 ± 0.6	4 #	68 ± 5	4 #	3.3 ± 0.1
AAt-CIII 24h-treated	-	-	61 ± 4	3.6 ± 0.2	2.67 ± 0.02

Table 1. **SANS data based structural parameters for cellulose I (CI) and cellulose III (CIII) controls and corresponding ex-situ A:At treated (for 24 h) samples are shown here.** Here, '#' denotes parameters that were fixed during the model fitting process.

pre-activated cellulose III, indicating a complete loss of the crystalline arrangement of the cellulose microfibril structure (**Figure 3B**). This observation implies that after 24 h of dissolution, A:At solvent had fully penetrated into the cellulose microfibrils and disrupted its core crystalline structure. Interestingly, the mid-*Q* R_g (60-68 Å) showed a marginal difference after A:At treatment. Unlike the features responsible for SANS signal in the high-Q region, the mid-Q feature represents larger cellulose structures. These larger entangled structures mostly arise upon precipitation of highly solvated cellulose chains from an A:At solution into an aqueous environment. Note that the larger cellulose structures detected in this Q-region do not need to be highly crystalline. However, in the high-Q region, the largest contrast is seen between cellulose structures with minimal solvent penetration and the solvent. Here, crystalline cellulose has the most contrast with respect to the solvent. In addition, the low-*Q* power-law exponent decreased from 3.3 ± 0.1 to 2.67 ± 0.02 after treatment of cellulose III by A:At solution. This change in the power-law exponent suggests that the amorphous cellulose recovered after A:At treatment has significantly higher solvent penetration and sufficiently disrupted microfibril structure.[51] This smaller power-law exponent qualitatively explains why A:At treated cellulose III results in a substrate with significantly higher rates of enzymatic hydrolysis unlike A:At treated cellulose I.

Mechanism of cellulose dissolution in A:At solvent system

Since A:At treatment *duration* had a critical impact on the recalcitrance of the recovered regenerated cellulose after pretreatment, it was necessary to carefully study the subtle structural changes in cellulose *in-situ* during the A:At treatment process using SANS (**Figure 4**). Ex-situ analysis revealed that the native allomorphs microfibril size (R_g) is 20 ± 1 Å and 18.6 ± 0.6 Å for Avicel based cellulose I and cellulose III, respectively (**Table 1**). These sizes are consistent with literature reported size of R_g =18.5 ± 0.5 Å for Avicel PH-105 microcrystalline cellulose.[44,51] In addition, the cellulose microfibril bundles in the mid-*Q* region are also of similar sizes, R_g ~ 60 ± 10 and 68 ± 5 Å, for cellulose I and cellulose III, respectively. The only clear distinction between cellulose I and cellulose III structures is the power-law exponent in the tertiary region, 4.0 ± 0.1 and 3.3 ± 0.1, respectively. Cellulose III exhibits a high degree of surface roughness of the large structures unlike the smoother surfaces of cellulose I. However, current set of *ex-situ* SANS analysis of recovered cellulose after A:At pretreatment provide limited mechanistic information on how subtle differences in cellulose structure impacts real-time A:At penetration and subsequent dissolution of pre-activated cellulose III. Therefore, we used SANS to characterize the ultrastructure of cellulose during real-time, *in-situ* dissolution using deuterated A:At solvent over a duration of 0-72 h at room temperature (**Figure 4**).

Structural parameters of the *in-situ* A:At treated cellulose was obtained from unified fit models of SANS data as before (**Table 2**). For cellulose I, the size of cellulose microfibrils marginally increased from 20 to 23-25 Å within 24 h of

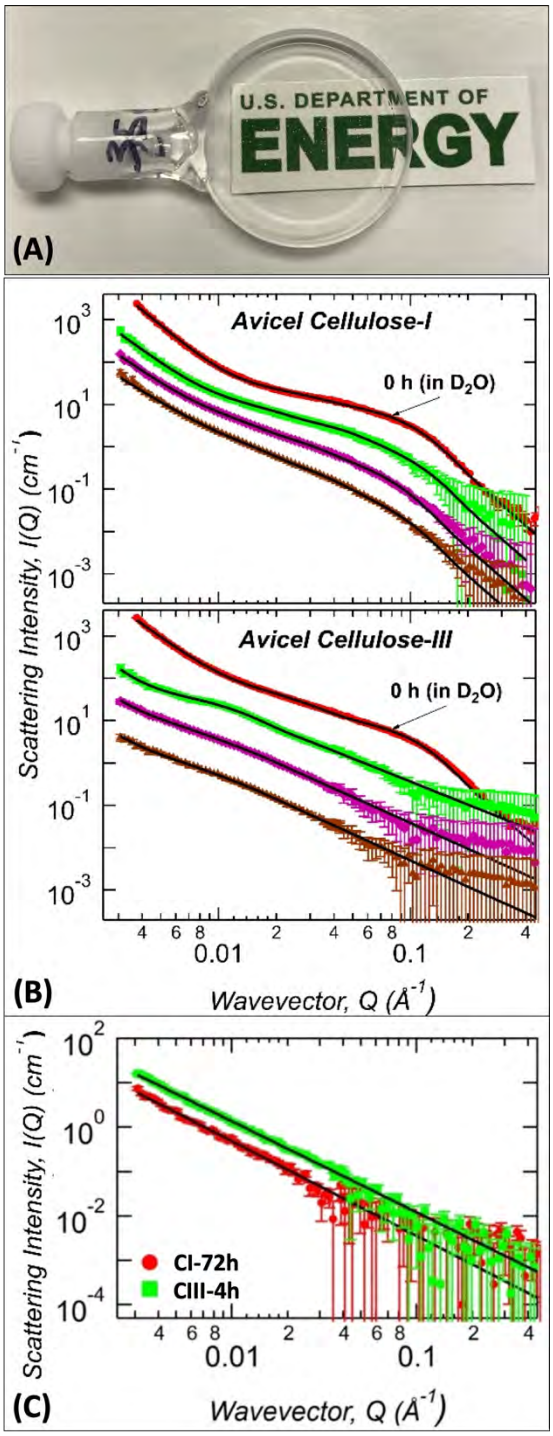

Figure 4. **In-situ ammonia:ammonium thiocyanate (A:At) dissolution of cellulose and characterization by Small Angle Neutron Scattering (SANS).** (A) Visual example SANS sample holder cell containing a clear solution of 2% (w/v) cellulose dissolved in deuterated A:At solution prepared using pre-activated cellulose III. (B) SANS profiles snapshot of untreated and deuterated A:At solvent treated (top) cellulose-I and (bottom) cellulose-III samples dissolved real-time for varying time periods. The curves are untreated controls are suspended in 100% D_2O (red dot); deuterated A:At solvent treated for 0.5 h (green square), 4 h (magenta diamond), and 24 h (brown up triangle) are shown here. The scattering curves are vertically shifted for clarity. (C) SANS profiles snapshot of protiated A:At solvent treated (green square) cellulose-I after 72 h and (red dot) cellulose-III samples after 4 h dissolution times, respectively. In all plots, solid black lines are the Unified fits to the experimental SANS data with results shown in Table 2.

Sample Type	High-Q R_g (Å)	High-Q Exponent, *P*	Mid-Q R_g (Å)	Mid-Q Exponent, *P*	Low-Q Exponent, *P*
		Avicel Cellulose- I			
In 100% D_2O	20 ± 1	4 #	60 ± 10	4 #	4.0 ± 0.1
0.5 h in ND_3:ND_4SCN	20 ± 3	4 #	80 ± 16	4 #	3.4 ± 0.2
4 h in ND_3:ND_4SCN	25 ± 3	4 #	110 ± 16	4 #	3.2 ± 0.1
24 h in ND_3:ND_4SCN	23 ± 2	4 #	94 ± 8	4 #	2.8 ± 0.1
72 h in NH_3:NH_4SCN*	-	-	-	2.05 ± 0.03	-
		Avicel Cellulose- III			
In 100% D_2O	18.6 ± 0.6	4 #	68 ±5	4 #	3.3 ± 0.1
0.5 h in ND_3:ND_4SCN	-	-	153 ± 6	1.8 ± 0.1	-
4 h in ND_3:ND_4SCN	-	-	280 ± 32	2.0 ± 0.1	-
24 h in ND_3:ND_4SCN	-	-	300 ± 41	2.1 ± 0.1	-
4 h in NH_3:NH_4SCN*	-	-	-	2.14 ± 0.07	-

Table 2. **SANS data based structural parameters for in-situ real-time dissolution of cellulose I (CI) and cellulose III (CIII) in deuterated and protiated* A:At solvents for varying durations of treatment time are shown here.** Here, '#' denotes parameters that were fixed during the model fitting process.

treatment (high-*Q* region). However, most of this change occurred after the first few hours of treatment. Cellulose bundles (or aggregates) increased mostly within the first 4 h of treatment (mid-*Q* region) and bundle associated R_g value remained constant up to 24 h. The surface morphology of the larger structures showed a gradual surface roughening during the treatment as indicated by the steady decrease in the low-*Q* power-law exponent. However, after 24 h of treatment, A:At had only penetrated the large structures of native cellulose I, which was sufficient to distinguish the highly entangled larger network from the intact crystalline core.

Cellulose III, unlike cellulose I, undergoes rapid deconstruction upon contact with A:At solvent. The cellulose microfibril feature in the high-*Q* region is not present within 30 min of treatment suggesting that A:At solvent readily penetrates and rapidly swells the cellulose crystalline core microfibrils. As a consequence, the microfibril features are not at all visible. Only changes in the cellulose bundle size (based on observed mid-*Q* R_g values) is observed likely due to rearrangement of the cellulose microfibrils within the bundles. Cellulose III bundle size increased by 100% from 0.5 h to 24 h of A:At treatment. A similar change in mid-*Q* R_g values is observed as seen earlier for cellulose-I. However, most of this change occurs within the first 4 h of treatment (i.e., 153 to 300 Å) and the bundles are much larger in size than those observed with cellulose I (i.e., 94 to 110 Å). In agreement with the trend seen for the radius of gyration, the bulk morphology obtained from the mid-*Q* exponent *P* suggests that the cellulose microfibril conformation transitions from a slightly stiff to flexible conformation at 0.5 h to 24 h, i.e., 1.8 to 2.1.[42] At the beginning of the treatment (~0.5 h), the thiocyanate anions are likely associated with the surface of closely-packed individual cellulose strands, thus inducing self-repulsion between cellulose-ion clusters to give rise to a stiffer polymer conformation. As the treatment proceeds, increasing solvation and A:At solvent penetration are expected to occur along with slow diffusion of the solvated cellulose chains into the bulk solvent, thereby making the cellulose chains dispersed in the solvent to be progressively more random oriented and thus have increased conformational flexibility.

The cellulose C6-hydroxymethyl group conformation likely plays a critical role on facilitating the rapid cellulose III microfibrils dissolution and ultimately aiding the solvation of individual cellulose polymer chains in A:At based solvent (**Figure 5**). We further hypothesize that individual solvated cellulose chains likely adopt a predominantly Gauche-Gauche (GG) and GT conformations due to strong hydrogen-bonding with cation-anion clusters that facilitate extensive cellulose solvation and prevent recrystallization of fully solvated cellulose polymer chains. Molecular dynamics simulations were carried out to test this hypothesis, characterize the hydrogen bonding interactions between cellulose-A:At, and gain understanding of the molecular mechanism of model cellulose polymer chain (i.e., cellohexaose) solvation in an A:At solvent. We found individually solvated cellohexaose chains adopt both Gauche-Trans (GT) and Gauche-Gauche (GG) hydroxymethyl conformations in A:At solvent due to strong interactions of cellulose with the ammonium cations that completely disrupt intrachain cellulose O2-O6 hydrogen bonding (**ESI Table S5**). The simulations also reveal the formation of ammonium cation/ammonia cationic clusters in the solvent that facilitated dissolution of solvated cellulose fibrils. Raman spectroscopic analysis for concentrated A:At solutions also revealed the presence of strong interactions of thiocyanate-ammonia and thiocyanate-ammonium ions,[52] which further validate our MD simulation findings. The strong interactions of cellulose with the A:At solvent facilitate extensive cellulose solvation and likely prevent recrystallization of fully solvated cellulose polymer chains. See ESI appendix for details (**ESI M5, Figures S5-S12 & Tables S5**). Finally, the MD simulation results support earlier hypothesis that dissolution of cellulose in ammonia-salt solutions would depend on the physical properties of the associated salt (e.g., anion size, solvation sphere, strength of interaction between ammonia and salt ions). Therefore, this suggests that the alternative ammonia-salt conditions with appropriate physical properties (e.g., ammonium iodide) might

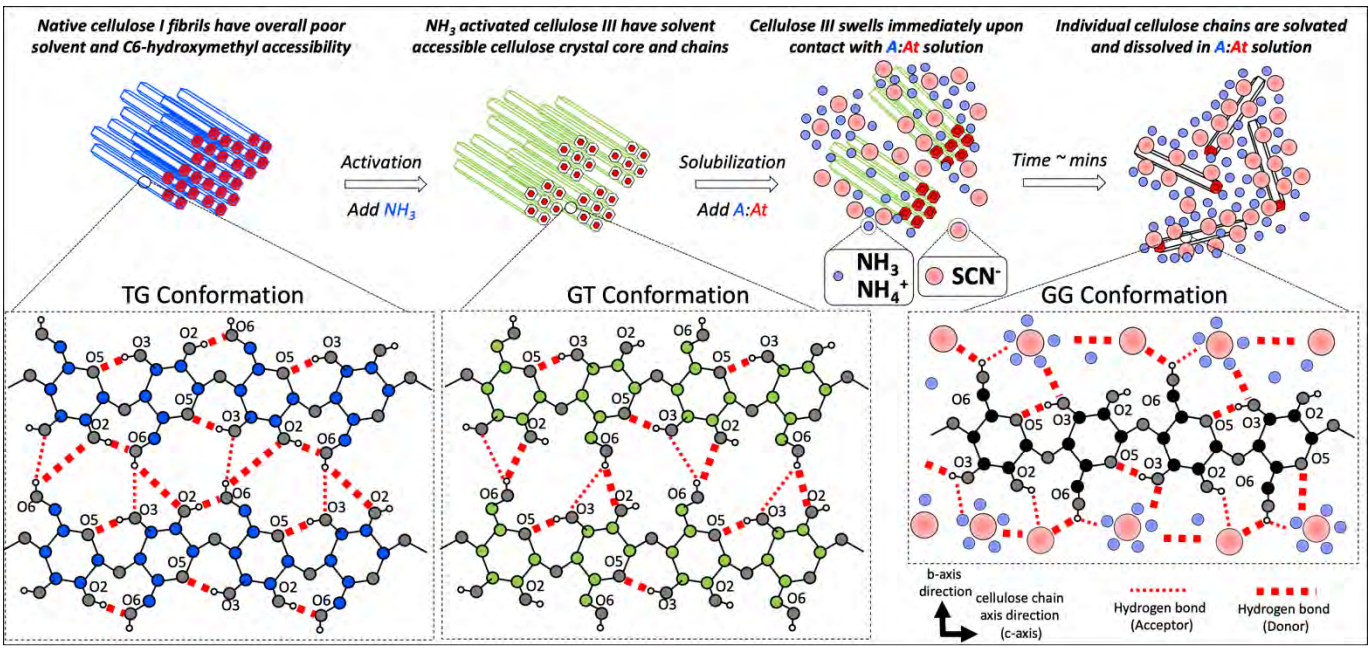

Figure 5. **Hypothesized role of cellulose C6-hydroxymethyl group conformation on rapid microfibrils dissolution and ultimately solvation of individual cellulose polymer chains in an ammonia:ammonium thiocyanate (A:At) based solvent.** Native cellulose I fibrillar structure is resistant to rapid dissolution in A:At largely due to a Trans-Gauche (TG) conformation of the C6-hydroxymethly group. However, ammonia pre-activation results in the formation of a slightly less tightly packed crystalline allomorph (i.e., cellulose III), with a predominantly Gauche-Trans (GT) conformation of the C6-hydroxymethyl group, and reduced intra-sheet hydrogen bonding. The GT-conformation and the altered accessible crystal morphology facilitates A:At solvent penetration into the core crystalline matrix and causes rapid swelling of the microfibrils. Finally, we hypothesize that individual solvated cellulose chains adopt a predominantly Gauche-Gauche (GG) and GT conformations due to strong hydrogen-bonding with ammonia/ammonium cation solvated thiocyanate ionic clusters that facilitates extensive solvation and prevents recrystallization of fully solvated cellulose polymer chains. Here, key cellulose intrasheet based interchain and intrachain hydrogen bonding (shown as dotted red lines for likely donor and/or acceptor bonds formed) for native cellulose Iβ, cellulose III, or soluble single cellulose chains is depicted in the dotted inset boxes with carbon atoms depicted in blue, green, or black filled circles, respectively. Oxygen and select hydrogen atoms are depicted as gray and white filled circles, respectively. Oxygen atoms are numbered according to the attached carbon atom. Ammonia/ammonium cations and thiocyanate anions are depicted by light blue and light red filled circles, respectively. Please note that all elements depicted in the schematic are not representative of actual relative scale.

be also able to dissolve rapidly cellulose if the cellulose has been pre-activated by ammonia.

Lastly, we have analyzed the *in-situ* SANS profiles for cellulose I dissolved in protiated A:At solvent after 3 days. Interestingly, the high-*Q* cellulose microfibril features and cellulose bundle features were not observed for either 4 h and 72 h A:At treated cellulose III and cellulose I, respectively (**Figure 4C**). However, the use of protiated solvents makes it difficult to resolve smaller structures. The reason is that the signal of cellulose microfibril and bundles/aggregates is reduced due to lower contrast. Also, incoherent background scattering from the hydrogen atoms in the system is significantly increased which makes the overall signal-to-noise rather poor. Nevertheless, the mid-Q exponent values of 2.05 observed suggests that significant disruption takes place in the cellulose I structure only after extended duration of incubation with the A:At solvent unlike pre-activated cellulose III.

One of the other limitations of the previous experimental approach to validate the polymorph interconversion process to explain the mechanism of cellulose I dissolution in A:At solvent was the regenerated cellulose samples analysis recovered after each A:At thermal cycle treatment step using XRD or NMR.[32,33] However, no in-situ studies were conducted to study real-time cellulose dissolution dynamics in A:At solutions. Although, Groot and co-workers used static light scattering (SLS) to characterize the structure of dissolved cellulose to determine the polymer persistence length and characterize the cellulose structure upon being fully solvated in A:At solutions.[39,53] But one of the major challenges associated with light scattering methods is the weak scattering observed due to the very low contrast in the refractive index of A:At and cellulose that ultimately resulted in radius of gyration (R_g) measurements with poor accuracy (±30-50% error) and low reliability since the R_g values estimated were close to the lower detection limit of classical SLS methods (~15 nm). Nevertheless, the radius of gyration predicted using SLS was predicted to be about ~21±11 nm for model cellulose fully dissolved in A:At solution. SANS is an effective alternative technique for dynamic multilength scale *in-situ* or static multilength scale *ex-situ* characterization of complex ultrastructures within highly heterogenous samples like cellulose or even whole plant cell walls.[54,55] We have now used deuterated A:At based solutions to overcome limitations associated with the poor contrast between the solvent and cellulose for maximizing the signal collected during neutron scattering. Real-time SANS characterization of dissolution of pre-activated cellulose III has revealed that the cellulose microfibril features are lost within a few minutes and the final radius of gyration (mid-Q range R_g) obtained within a few hours was stabilized at about ~29±5 nm. These values are consistent with observations made for molecular solutions of cellulose for other solvents like IL.[55–57]

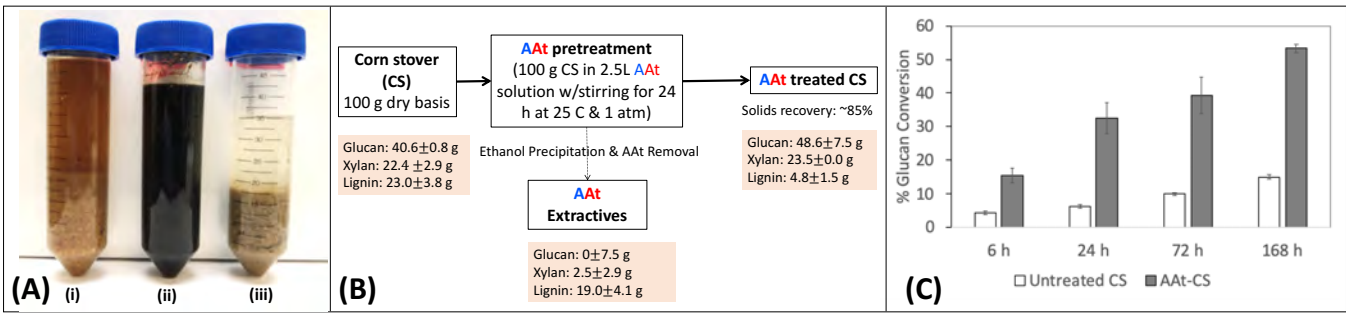

Figure 6. **Lignocellulosic biomass ambient conditions pretreatment and selective lignin fractionation using an ammonia:ammonium thiocyanate (A:At) based solvent system.** (A) Representative images of corn stover (CS) suspended in water (i), A:At solvent during treatment (ii), and after ethanol precipitation for dissolved solids recovery (suspended here in 100% ethanol) (iii). (B) Mass balance and composition analysis (i.e., glucan, xylan, and total lignin) for corn stover before and after A:At pretreatment are shown here. Here, all mass balance and compositional analysis experiments were done in two replicate batches conducted on two separate days each (see ESI M4 for details) and the relevant mean values and corresponding standard deviations are reported here. The A:At CS extractives composition was indirectly estimated based on the untreated CS and A:At CS substrate composition as well as based on the ~85% solids mass recovery values. (C) Cellulase activity assay studies reveal that A:At treated corn stover gives higher cellulose hydrolysis yields versus untreated corn stover during all saccharification time points.

Lignocellulosic biomass pretreatment under ambient conditions

Finally, we were interested in generating proof-of-concept data to show that the A:At solvent system could be used to directly pretreat and fractionate lignocellulosic biomass like corn stover into its constituent components similar to other reported IL. Interestingly, addition of untreated corn stover to A:At solvent almost instantly gave rise to a dark brown colored and slightly viscous gel-like solution (**Figure 6A**). Corn stover was incubated at 4% (w/v) solids loading in the A:At solvent under ambient conditions for 24 h prior to addition of ethanol as anti-solvent to precipitate any solubilized polysaccharides to perform a material balance analysis. The supernatant was then removed after centrifugation and the solid biomass pellet was washed to remove any residual A:At. We found about ~15-20% of the starting material by weight was extracted from corn stover by A:At solvent (**Figure 6B**). Compositional analysis revealed that A:At solvent was able to readily extract close to ~80-85% of original available total lignin, while leaving behind most of the polysaccharides (i.e., glucans and xylans) largely intact with significantly less than ~5% total sugar loss in the extractives stream. Overall lignin extraction yields for the A:At solvent based biomass pretreatment process were nearly double of our previous reported value for the EA process (~40%),[24] but with similar polysaccharide extraction yields. However, unlike the current proposed A:At pretreatment process performed at 25 °C and ~15 psi pressure, the EA process was operating at a much higher thermochemical severity (e.g., ~100-130 °C at ~1200-1500 psi operational pressures). Furthermore, the A:At solvent pretreated residual corn stover polysaccharides were shown to be readily hydrolyzed using a low enzyme loading (~2 mg/g glucan) into soluble sugars like glucose (**Figure 6C**). There is obviously room for further process improvement as no optimization has been currently performed on either the solvent system composition or exact pretreatment conditions that maximize treated cellulosic biomass conversion yields.

Conclusions

Saturated solutions of ammonia-ammonium thiocyanate (A:At) were first reported as a possible non-derivatizing solvent system to fully dissolve regenerated amorphous cellulose, like viscose cellulose, by Scherer in 1931.[30] However, mixed results were reported for the dissolution ability of several ammonia-salt solutions on more crystalline forms of cellulose like cotton. It was only half a century later in the 1980's that Cuculo and co-workers at North Carolina State University developed a multi-stage thermal cycling based treatment process using extremely low freezing temperatures to more effectively dissolve crystalline cellulose like cotton linters into A:At type solvents.[31] This process involved exposing the cellulose to A:At solvent first to a low freezing temperature (e.g., -80 to -20 °C) for several hours to days followed by slowly bringing the temperature up to 20-40 °C with constant mechanical stirring. The low temperature cycle process was then repeated again multiple times to facilitate complete dissolution. Cuculo and co-workers hypothesized about the mechanism of native crystalline cellulose I dissolution in A:At solvent, due to extreme thermal cycling steps, took place via intermediate polymorph transformations similar in structures to cellulose II and III.[32,33] They invoked the interplay of entropic vs. enthalpic thermodynamic effects driving ammonia-thiocyanate vs. ammonia-cellulose interactions at the extreme ranges of the thermal cycling temperatures to rationalize the polymorph transformation mechanism. *However, the critical role of the cellulose ultrastructure modification to either cellulose-ammonia complex, or cellulose III allomorph, on the real-time dissolution kinetics of cellulose in A:At solvent was not explored.* We have now shown that pre-activation of cellulose by ammonia to form a metastable cellulose-ammonia complex, or cellulose III allomorph, facilitates near-instantaneous swelling and penetration of A:At solution to rapidly dissolve cellulose within a few mins. Furthermore, this pre-activation step allows cellulose dissolution at near ambient conditions with no requirement for extreme thermal cycling temperatures or extensive mechanical mixing of the cellulose solution. Molecular dynamics simulations provided detailed insight into the highly dynamic hydrogen bonding interactions between cellulose and ammonium cation/ammonia cationic clusters that

disrupted intramolecular cellulose hydrogen bonds. Our MD analysis also provides further support to the polymorph interconversion hypothesis that explains why pre-activated cellulose III like allomorphs are rapidly solvated and fully dissolved in A:At type solvents unlike cellulose I at room temperature without any necessity for extensive thermal cycling.

We have also conducted detailed enzymatic assays to show that amorphous cellulose regenerated from a molecular solution of A:At prepared using pre-activated cellulose III can be rapidly digested by cellulases at ultra-low enzyme loadings (0.1-1 mg/g glucan) to soluble sugars like glucose, unlike native crystalline cellulose I and cellulose III as well. Also, we have confirmed A:At based solvents can selectively extract lignin from complex lignocellulosic biomass like corn stover while significantly reducing recalcitrance of residual polysaccharides to enzymatic hydrolysis even at low enzyme loadings. The proposed A:At pretreatment process can be theoretically conducted at ambient conditions unlike the traditional EA or other anhydrous liquid ammonia based pretreatments. Compared to ionic liquids like 1-ethyl-3-methylimidazolium acetate, the dynamic viscosity of the A:At solution alone is nearly 3 orders of magnitude lower under comparable process conditions (see **ESI M6** for detailed analysis of A:At solvent and A:At/cellulose solution viscosity). This clearly highlights that A:At solvent is an ideal low viscosity solvent for cellulose dissolution at room temperature unlike conventional ILs for cellulose pretreatment. Furthermore, since efficient cellulose deconstruction is likely dependent on the exact A:At processing conditions (e.g., cellulose loading, dissolution temperature, mixing/stirring/shear rate), we believe there is ample opportunity to further reduce total processing time (i.e., under 1 h) and solvent loading (i.e., by increasing cellulose loading) by further optimizing pretreatment conditions as well as optimizing enzymatic saccharification conditions to achieve near-theoretical hydrolysis yields similar to currently mature IL-based processes. Our promising lignocellulosic biomass fractionation-type pretreatment results inspire confidence about the possibility of selectively optimizing and upgrading the carbohydrate and aromatics enriched product streams into diverse bioproducts using either standalone or hybrid catalytic/biocatalytic processing routes in the near future. Cuculo and co-workers have already reported that A:At type solvents are non-derivatizing and do not cause any cellulose degradation upon long-term incubation with cellulose at temperatures close to 25 °C.[31,58] However, ammonia-based solvents/pretreatments (e.g., AFEX/EA) are reported to form minor glucosamine derivatives due to the reaction of ammonia with reducing sugar aldehydes as well as amides due to ammonolytic reactions of lignin-carbohydrate ester linkages.[24,59,60] It is currently unclear if A:At could further alter the core lignin structure during similar ammonolytic-type reactions (similar to AFEX[61] or EA[62] pretreatment) at room temperature during pretreatment that facilitates lignocellulose fractionation and how exactly such lignin structural modifications would impact either downstream fermentation process for sugar-upgrading or catalytic conversion processes for lignin valorization.

Regarding safety, health, and environmental or SH&E factors impacting overall 'sustainability', toxicity is indeed an important consideration for commercialization/scale-up of any biorefinery process employing chemicals. From a SH&E sustainability point of view, classical solvents (e.g., ethanol) have clear SH&E guidelines to allow ranking of such solvents as first reported in a 2016 *Green Chemistry* study,[63] but it is challenging to determine similar solvent ranking scores for poorly studied ionic liquids or chemically complex mixtures (e.g., A:At) based solvent systems. Nevertheless, based on the available Global Harmonized System (GHS) ratings, we can readily estimate the combined solvent/chemical SH&E ranking score for ammonium thiocyanate alone to be 8 (i.e., classified as hazardous based on the 2016 report for ranking solvent 'greenness' using a combined SH&E criteria score).[63] This poor ranking score is mostly based of an environmental criteria score of 5 due to the high aquatic environmental toxicity rating of ammonium thiocyanate (i.e., H412 GHS rating). Thus, an ammonia-salt solvent system employing ammonium thiocyanate as salt would likely be also classified as hazardous using similar SH&E criteria. However, we believe our current study provides a clear mechanistic basis for developing similar one-pot biomass fractionation by ammonia-salt solvent systems using alternative salts that have more favorable SH&E ratings (e.g., ammonium chloride or iodide). Ammonium iodide was originally also reported by Scherer in 1931,[30] along with ammonium thiocyanate, to also dissolve regenerated viscose cellulose in ammonia-salt solutions but ammonium iodide based solvents were reported to only have partial solubility for crystalline cotton cellulose. However, it is very likely that pre-activation of cellulose by ammonia alone would also facilitate dissolution of pre-activated crystalline cellulose III in ammonia-ammonium iodide solutions. While Cuculo and co-workers revisited the ammonia-ammonium thiocyanate solvent system for cellulose dissolution using an improved cellulose-solvent slurry freeze/thaw method in the 1980's,[31] no additional work has been reported in the open literature on the use of alternative ammonium salts for cellulose dissolution. Similarly, while ammonium chloride is known to also dissolve in liquid ammonia to form stable ammonia-salt solutions at room temperature,[64] no data is currently available on the suitability of an equivalent ammonia-ammonium chloride solvent system for enabling rapid cellulose dissolution. Detailed future studies would be necessary to explore alternative ammonium salts (e.g., ammonium iodides or chlorides) that are potentially less toxic and have better SH&E sustainability ratings than ammonium thiocyanate to be used in similar one-pot ammonia pre-activation based rapid cellulose dissolution process. For example, the current safety and health criteria score for ammonium chloride is 1 (due to its desired low flammability) and 2 (mostly due to its undesired acute toxicity upon oral ingestion), respectively. The GHS ratings for ammonium iodide (or chloride) suggest these alternative chemicals are less hazardous than ammonium thiocyanate and likely have a combined SH&E solvent rating criterion similar to other

ammonium or quaternary ammonium-based salts currently used in agricultural systems.[65] Furthermore, due to the world-wide prevalent use of ammonia and ammoniacal salts as fertilizers in our current agricultural systems, an appropriate choice of a suitable ammonia-salt system with ideal SH&E ratings would facilitate systematic integration of such chemicals into our current agro-industrial economy for large-scale implementation of ammonia/ammonia-salt based biorefineries.

Regarding technoeconomic factors impacting 'sustainability', our currently proposed approach from a process intensification point-of-view combines elements of a traditional AFEX or EA based pretreatment process along with Scherrer/Cuculo's reported ammonia-ammonium thiocyanate solvent system to achieve a new one-pot process with likely signification reduction in overall capital costs and/or energy usage for cost-effective conversion of cellulosic biomass to fermentable sugars in a biorefinery. We believe our proposed process simplification and pretreatment mechanism-based process intensification would lead to a more economic and energetically sustainable process. Reducing the overall thermal and pressure severity employed by use of ammonia-based solvents could promote development of more sustainable and safer processing strategies for biomass refining. Furthermore, ammonia-salt based solvents have a significantly lower cost than traditional ionic liquids which could also significantly lower the economic barrier for implementing such pretreatment processes in biorefineries. Recent work has focused on the development of low-cost ionic liquids to address this very issue for cellulosic biomass pretreatment. For example, quaternary ammonium salts[66] and lignin-derived bionic liquids[67] have been recently reported as alternative low-cost ionic liquids for biomass pretreatment. However, most previous work that have used such ionic liquids (e.g., triethylammonium hydrogen sulfate) often require elevated temperatures (i.e., 120-130 °C) for effective cellulosic biomass pretreatment due to the high viscosity of such solvent systems at lower temperatures. But we have shown it is possible to pretreat/fractionate lignocellulosic biomass at room temperature/pressure using our low-viscosity model ammonia-salt solvent system,[58] which could reduce safety related hazards associated with handling any solvents/chemicals at elevated temperatures. Nevertheless, a detailed technoeconomic and life cycle analysis of similar processes (including solvent recycle) will need to be pursued in the near future to properly evaluate the feasibility of ammonia-salt based solvents for commercial applications.

Author contributions

SPSC conceived the project. SPSC, LS, and RP prepared the ammonia-salt solutions. SPSC, LS, SVP, and HO carried out the SANS experiments; while ZY and SVP performed all SANS data analysis. SR, SG, and CZ performed all post-treatment sample characterization, enzymatic processing, and data analysis. SHL and LP performed the MD simulations and relevant data analysis. SPSC wrote the manuscript. All authors contributed to reviewing and editing the final paper.

Conflicts of interest

SPSC has filed for patent applications on processes to produce cellulose-III enriched cellulosic biomass for biofuels production (US20130244293A1 and WO2011133571A2). Other authors have no conflicts to declare.

Acknowledgements

SPSC acknowledges support from the ORAU 2016 Ralph E. Powe Award, ORNL Neutron Sciences User Facility, US National Science Foundation CBET awards (1604421 and 1846797), Rutgers Global Grant, Rutgers Division of Continuing Studies, Rutgers School of Engineering, and the Great Lakes Bioenergy Research Center (DOE BER Office of Science DE-FC02-07ER64494). MD and SANS studies on Bio-SANS were supported by the Office of Biological and Environmental Research (OBER) funded Center for Structural Molecular Biology (CSMB) under Contracts FWP ERKP291 and FWP ERKP752, using the High Flux Isotope Reactor supported by the Office of Basic Energy Sciences (BES), U. S. Department of Energy (DOE). SR and CZ acknowledge support from University Grants Commission of India (Raman Fellowship Program) and China Scholarship Council, respectively, to support their one-year postdoctoral research work at SPSC's lab at Rutgers University. Lastly, we are very grateful to Benjamin Esposito and Jia-Mei Hong from SPSC's Rutgers research group for their critical experimental contributions to the project.

This manuscript has been co-authored by UT-Battelle, LLC, under Contract No. DE-AC05-00OR22725 with the U.S. Department of Energy. The United States Government retains and the publisher, by accepting the article for publication, acknowledges that the United States Government retains a non-exclusive, paid-up, irrevocable, world-wide license to publish or reproduce the published form of this manuscript, or allow others to do so, for United States Government purposes. The Department of Energy will provide public access to these results of federally sponsored research in accordance with the DOE Public Access Plan (http://energy.gov/downloads/doe-public-access-plan).

References

1 G. T. Beckham, J. F. Matthews, B. Peters, Y. J. Bomble, M. E. Himmel and M. F. Crowley, *J. Phys. Chem. B*, 2011, **115**, 4118–4127.

2 P. J. Weimer, A. D. French and T. A. Calamari Jr., *Appl. Environ. Microbiol.*, 1991, **57**, 3101–3106.

3 S. P. S. Chundawat, G. Bellesia, N. Uppugundla, L. Sousa, D. Gao, A. Cheh, U. Agarwal, C. Bianchetti, G. Phillips, P. Langan, V. Balan, S. Gnanakaran and B. E. Dale, *J. Am. Chem. Soc.*, 2011, **133**, 11163–11174.

4 Y.-H. P. Zhang, S.-Y. Ding, J. R. Mielenz, J.-B. Cui, R. T. Elander, M. Laser, M. E. Himmel, J. R. McMillan and L. R. Lynd, *Biotechnol. Bioeng.*, 2007, **97**, 214–223.

5 F. Xu, J. Sun, N. V. S. N. M. Konda, J. Shi, T. Dutta, C. D. Scown, B. A. Simmons and S. Singh, *Energy Environ. Sci.*, 2016, **9**, 1042–1049.

6 J. S. Luterbacher, J. M. Rand, D. M. Alonso, J. Han, J. T. Youngquist, C. T. Maravelias, B. F. Pfleger and J. A. Dumesic, *Science*, 2014, **343**, 277–80.

7 M. Tyufekchiev, P. Duan, K. Schmidt-Rohr, S. Granados Focil, M. T. Timko and M. H. Emmert, *ACS Catal.*, 2018, **8**, 1464–1468.

8 T. Y. Nguyen, C. M. Cai, R. Kumar and C. E. Wyman, *ChemSusChem*, 2015, **8**, 1716–1725.

9 E. Johnson, *Biofuels, Bioprod. Biorefining*, 2016, **10**, 164–174.

10 D. Kumar and V. Singh, *Biotechnol. Biofuels*, 2016, **9**, 228.

11 T. Liebert, in *Cellulose Solvents: For Analysis, Shaping and Chemical Modification*, American Chemical Society, 2010, vol. 1033, pp. 3–54.

12 S. Singh and B. A. Simmons, in *Aqueous Pretreatment of Plant Biomass for Biological and Chemical Conversion to Fuels and Chemicals*, John Wiley & Sons, Ltd, 2013, pp. 223–238.

13 S. P. S. Chundawat, G. T. Beckham, M. Himmel and B. E. Dale, *Annu. Rev. Chem. Biomol. Eng.*, 2011, **2**, 121–145.

14 A. Pinkert, K. N. Marsh and S. Pang, *Ind. Eng. Chem. Res.*, 2010, **49**, 11121–11130.

15 D. Klein-Marcuschamer, B. A. Simmons and H. W. Blanch, *Biofuels, Bioprod. Biorefining*, 2011, **5**, 562–569.

16 L. Chen, M. Sharifzadeh, N. Mac Dowell, T. Welton, N. Shah and J. P. Hallett, *Green Chem.*, 2014, **16**, 3098.

17 H. Schleicher, C. Daniels and B. Philipp, *J. Polym. Sci. Part C-Polymer Symp.*, 1974, 251–260.

18 A. Mittal, R. Katahira, M. Himmel and D. Johnson, *Biotechnol. Biofuels*, 2011, **4**, 41.

19 A. J. Barry, F. C. Peterson and A. J. King, *J. Am. Chem. Soc.*, 1936, **58**, 333–337.

20 K. Igarashi, M. Wada and M. Samejima, *FEBS J.*, 2007, **274**, 1785–1792.

21 M. Lewin and L. G. Roldan, *J. Polym. Sci. Part C-Polymer Symp.*, 1971, 213–229.

22 W. E. Davis, A. J. Barry, F. C. Peterson and A. J. King, *J. Am. Chem. Soc.*, 1943, **65**, 1294–1299.

23 G. L. Clark and E. A. Parker, *J. Phys. Chem.*, 1937, **41**, 777–786.

24 L. da Costa Sousa, M. Jin, S. P. S. Chundawat, V. Bokade, X. Tang, A. Azarpira, F. Lu, U. Avci, J. Humpula, N. Uppugundla, C. Gunawan, S. Pattathil, A. M. Cheh, N. Kothari, R. Kumar, J. Ralph, M. G. Hahn, C. E. Wyman, S. Singh, B. A. Simmons, B. E. Dale and V. Balan, *Energy Environ. Sci.*, 2016, **9**, 1215–1223.

25 E. Sendich, M. Laser, S. Kim, H. Alizadeh, L. Laureano-Perez, B. Dale and L. Lynd, *Bioresour. Technol.*, 2008, **99**, 8429–8435.

26 L. Tao, A. Aden, R. T. Elander, V. R. Pallapolu, Y. Y. Lee, R. J. Garlock, V. Balan, B. E. Dale, Y. Kim, N. S. Mosier, M. R. Ladisch, M. Falls, M. T. Holtzapple, R. Sierra, J. Shi, M. A. Ebrik, T. Redmond, B. Yang, C. E. Wyman, B. Hames, S. Thomas and R. E. Warner, *Bioresour. Technol.*, 2011, **102**, 11105–14.

27 L. da C. Sousa, J. Humpula, V. Balan, B. E. Dale and S. P. S. Chundawat, *ACS Sustain. Chem. Eng.*, 2019, **7**, 14411–14424.

28 H. W. Foote and M. A. Hunter, *J. Am. Chem. Soc.*, 1920, **42**, 69–78.

29 S. P. S. Chundawat, B. Bals, T. Campbell, L. Sousa, D. Gao, M. Jin, P. Eranki, R. Garlock, F. Teymouri, V. Balan and B. E. Dale, in *Aqueous Pretreatment of Plant Biomass for Biological and Chemical Conversion to Fuels and Chemicals*, John Wiley & Sons, Ltd, 2013, pp. 169–200.

30 P. C. Scherer, *J. Am. Chem. Soc.*, 1931, **53**, 4009–4013.

31 S. M. Hudson and J. A. Cuculo, *J. Polym. Sci. Polym. Chem. Ed.*, 1980, **18**, 3469–3481.

32 J. A. Cuculo, C. B. Smith, U. Sangwatanaroj, E. O. Stejskal and S. S. Sankar, *J. Polym. Sci. Part A Polym. Chem.*, 1994, **32**, 241–247.

33 J. A. Cuculo, C. B. Smith, U. Sangwatanaroj, E. O. Stejskal and S. S. Sankar, *J. Polym. Sci. Part A Polym. Chem.*, 1994, **32**, 229–239.

34 G. Bellesia, S. P. S. Chundawat, P. Langan, B. E. Dale and S. Gnanakaran, *J. Phys. Chem. B*, 2011, **115**, 9782–9788.

35 R. Parthasarathi, G. Bellesia, S. P. S. Chundawat, B. E. Dale, P. Langan and S. Gnanakaran, *J. Phys. Chem. A*, 2011, **115**, 14191–14202.

36 G. Bellesia, S. P. S. Chundawat, P. Langan, A. Redondo, B. E. Dale and S. Gnanakaran, *J. Phys. Chem. B*, 2012, **116**, 8031–8037.

37 D. Sawada, L. Hanson, M. Wada, Y. Nishiyama and P. Langan, *Cellulose*, 2014, **21**, 1117–1126.

38 Y. Li, J. Wang, X. Liu and S. Zhang, *Chem. Sci.*, 2018, **9**, 4027–4043.

39 A. W. De Groot, D. E. Guinnup, M. H. Thiel and J. A. Cuculo, *J. Polym. Sci. Part B Polym. Phys.*, 1991, **29**, 557–563.

40 G. W. Lynn, W. Heller, V. Urban, G. D. Wignall, K. Weiss and D. A. A. Myles, *Phys. B Condens. Matter*, 2006, **385**–**386**, 880–882.

41 J. Ilavsky and P. R. Jemian, *J. Appl. Crystallogr.*, 2009, **42**, 347–353.

42 G. Beaucage, *J. Appl. Crystallogr.*, 1996, **29**, 134–146.

43 G. Beaucage, *J. Appl. Crystallogr.*, 1995, **28**, 717–728.

44 S. V. Pingali, V. S. Urban, W. T. Heller, J. McGaughey, H. M. O'Neill, M. Foston, D. A. Myles, A. J. Ragauskas and B. R. Evans, *Acta Crystallogr. Sect. D Biol. Crystallogr.*, 2010, **66**, 1189–1193.

45 S. P. S. Chundawat, V. Balan and B. E. Dale, *Biotechnol. Bioeng.*, 2008, **99**, 1281–1294.

46 S. P. S. Chundawat, M. S. Lipton, S. O. Purvine, N. Uppugundla, D. Gao, V. Balan and B. E. Dale, *J. Proteome Res.*, 2011, **10**, 4365–4372.

47 M. G. Resch, J. O. Baker and S. R. Decker, *Tech. Rep. NREL/TP-5100-63351, Lab. Anal. Proced.*, 2015, 1–9.

48 D. Gao, S. P. S. Chundawat, C. Krishnan, V. Balan and B. E. Dale, *Bioresour. Technol.*, 2010, **101**, 2770–2781.

49 N. Sathitsuksanoh, Z. Zhu, S. Wi and Y. H. Percival Zhang, *Biotech Bioeng*, 2011, **108**, 521–529.

50 S. Bhagia, R. Dhir, R. Kumar and C. E. Wyman, *Sci. Rep.*, 2018, **8**, 1350.

51 S. V. Pingali, V. S. Urban, W. T. Heller, J. McGaughey, H. O'Neill, M. Foston, D. A. Myles, A. Ragauskas and B. R. Evans, *Biomacromolecules*, 2010, **11**, 2329–2335.

52 A. T. Lemley and J. J. Lagowski, *J. Phys. Chem.*, 1974, **78**, 708–713.

53 A. W. De Groot, D. E. Guinnup, M. H. Theil and J. A. Cuculo, *J. Polym. Sci. Part B Polym. Phys.*, 1991, **29**, 547–556.

54 G. Cheng, X. Zhang, B. Simmons and S. Singh, *Energy Environ. Sci.*, 2015, **8**, 436–455.

55 V. S. Raghuwanshi, Y. Cohen, G. Garnier, C. J. Garvey, R. A. Russell, T. Darwish and G. Garnier, *Macromolecules*, 2018, **51**, 7649–7655.

56 D. M. Rein, R. Khalfin, N. Szekely and Y. Cohen, *Carbohydr. Polym.*, 2014, **112**, 125–133.

57 M. Yang, W. Zhao, S. Wang, C. Yu, S. Singh, B. Simmons and G. Cheng, *Cellulose*, 2019, **26**, 2243–2253.

58 S. M. Hudson, J. A. Cuculo and L. C. Wadsworth, *J. Polym. Sci. Polym. Chem. Ed.*, 1983, **21**, 651–670.

59 A. W. Degroot, F. I. Carroll and J. A. Cuculo, *J. Polym. Sci. Part A Polym. Chem.*, 1986, **24**, 673–680.

60 S. P. S. Chundawat, R. Vismeh, L. Sharma, J. Humpula, L. Sousa, C. K. Chambliss, A. D. Jones, V. Balan and B. E. Dale, *Biores Technol*, 2010, **101**, 8429–8438.

61 S. P. S. Chundawat, B. S. Donohoe, L. Sousa, T. Elder, U. P. Agarwal, F. Lu, J. Ralph, M. E. Himmel, V. Balan and B. E. Dale, *Energy Environ. Sci.*, 2011, **4**, 973–984.

62 L. da Costa Sousa, M. Foston, V. Bokade, A. Azarpira, F. Lu, A. J. Ragauskas, J. Ralph, B. Dale and V. Balan, *Green Chem.*, 2016, **18**, 4205–4215.

63 D. Prat, A. Wells, J. Hayler, H. Sneddon, C. R. McElroy, S. Abou-Shehada and P. J. Dunn, *Green Chem.*, 2016, **18**, 288–296.

64 H. Hunt and L. Boncyk, *J. Am. Chem. Soc.*, 1933, **55**, 3528–3530.

65 EPA-SAB, *Reactive Nitrogen in the United States: An Analysis of Inputs, Flows, Consequences, and Management Options. A Report of the EPA Science Advisory Board*, Washington, DC, 2011.

66 A. George, A. Brandt, K. Tran, S. M. S. N. S. Zahari, D. Klein-Marcuschamer, N. Sun, N. Sathitsuksanoh, J. Shi, V. Stavila, R. Parthasarathi, S. Singh, B. M. Holmes, T. Welton, B. A. Simmons and J. P. Hallett, *Green Chem.*, 2015, **17**, 1728–1734.

67 A. M. Socha, R. Parthasarathi, J. Shi, S. Pattathil, D. Whyte, M. Bergeron, A. George, K. Tran, V. Stavila, S. Venkatachalam, M. G. Hahn, B. A. Simmons and S. Singh, *Proc. Natl. Acad. Sci. U. S. A.*, 2014, **111**, E3587–E3595.

Electronic Supplementary Information (ESI) Document:

Ammonia-salt solvent promotes cellulosic biomass deconstruction under ambient pretreatment conditions to enable rapid soluble sugar production at ultra-low enzyme loadings

Shishir P. S. Chundawat,[a]* Leonardo da Costa Sousa,[b] Shyamal Roy,[a,c] Zhi Yang,[d] Shashwat Gupta,[a] Ramendra Pal,[e] Chao Zhao,[a,f] Shih-Hsien Liu,[g] Loukas Petridis,[g] Hugh O' Neill,[d] Sai Venkatesh Pingali[d]

a) *Department of Chemical & Biochemical Engineering, Rutgers The State University of New Jersey, Piscataway, NJ 08854, USA. *Corresponding Author Email: shishir.chundawat@rutgers.edu*
b) *Department of Chemical Engineering & Materials Science, Michigan State University, East Lansing, MI 48824, USA.*
c) *Department of Chemical Engineering, Jadavpur University, Jadavpur, Kolkata, West Bengal 700032, India. (Current Address)*
d) *Center for Structural Molecular Biology, Oak Ridge National Laboratory, Oak Ridge, TN 37831, USA.*
e) *Department of Mechanical & Aerospace Engineering, Rutgers The State University of New Jersey, Piscataway, NJ 08854, USA.*
f) *School of Engineering, Zhejiang A&F University, Linan, Zhejiang 311300, People's Republic of China. (Current Address)*
g) *UT/ORNL Center for Molecular Biophysics, Oak Ridge National Laboratory, Oak Ridge, Tennessee 37831, USA.*

Number of Pages: 29
Number of Figures: 13
Number of Tables: 5
Number of Movies: 1

ESI Methods & Results Section:

M1. X-ray diffraction (XRD) method and data analysis

XRD was performed on a Philips X'Pert X-ray Powder Diffractometer (Malvern Panalytical Ltd., Royston, UK). CuKα radiation (wavelength = 1.5418 Å) was generated at 40 kV and 40 mA. Detector slit was set to 0.3 mm. Sample was analyzed using a coupled 2θ/θ scan type with a continuous PSD fast scan mode. The 2θ started at 3° and ended at 90° with a step size of 0.02° and time step of 3 seconds per step. Lyophilized cellulose samples (approximately 0.3 g) were placed in a rotating specimen holder ring (4 secs/revolution).

Cellulose crystallinity index (CrI), for Avicel based cellulose I and III allomorphs, was quantified based on two different methods, namely; XRD peak height and peak deconvolution methods, as highlighted elsewhere.[1,2] For the XRD peak height method, CrI was calculated from the ratio of the height of the 002 peak (I_{002}) and the height of the minimum (I_{AM}) between the 002 and 101 peaks ($CrI = 100*(I_{002}-I_{AM})/I_{002}$). The I_{002} and I_{AM} peaks for cellulose I were at 22.5° and 18.6°, while for cellulose III they were at 20.7° and 17.8°, respectively. The CrI estimated based on the peak height method for cellulose I and III controls were 84% and 79%, respectively. For the XRD peak deconvolution method, peak deconvolutions were carried out using PeakFit software (Version 4.12, Systat Software Inc, San Jose, CA) as described elsewhere.[2] For all peak deconvolutions F values are always > 15,000 while R-squares > 0.99. For cellulose I and all relevant ammonia:ammonium thiocyanate or A:At treated cellulose-I samples, five crystalline peaks (at 14.76°, 16.38°, 20.53°, 22.40°, and 34.34°) and one amorphous peak (21.5°) were deconvoluted and fitted to the original XRD spectra. For cellulose III and relevant A:At treated cellulose-III samples, six crystalline peaks (at 11.65°, 17.1°, 20.62°, 28.21°, 34.60°, and 35.95°) and one amorphous peak (21.5°) were deconvoluted and fitted to the original spectra. CrI based on peak deconvolution method was estimated by taking the percent ratio of the crystalline peak area (AC) to the total area (AT) of all deconvoluted peaks ($CrI= 100*AC/AT$). The CrI for cellulose I and III controls were 66% and 58%, respectively. The average crystallite size was next estimated based on the width of the most intense deconvoluted crystalline peak (e.g., 002 reflection) at half height using the Scherrer equation ($D = 57.3K\lambda/(\beta \cos(\theta))$).[3] Where; D is the average dimension of the crystallite area measured vertically to the corresponding reflecting lattice plane, K is the form factor constant equal to 0.89, λ is the wavelength of the incident X–ray equal to 1.5418 Å, 57.3 is the conversion factor for degrees to radians, θ is the Bragg diffraction angle of X–rays on the plane under consideration, and β is the full width half maximum of the X–ray peak corresponding to the 002 peak. Average size of the Avicel derived cellulose I and III control crystallites corresponding to the respective deconvoluted 002 peaks were 5.1 and 4.2 nm, respectively. Note that for 6 h and 24 h A:At treated cellulose III, only three peaks (at ~22°, ~28°, ~34°) could be deconvoluted and fitted to the highly amorphous XRD spectra. Therefore, crystallite size analysis for 6 h and 24 h A:At treated cellulose III was performed using the dominant broad amorphous peak at ~22° for sake of comparison with other treated samples.

M2. Scanning Electron Microscopy (SEM) analysis

SEM analyses on all lyophilized cellulose samples were performed using a Zeiss Sigma field emission SEM (Carl Zeiss Microscopy, Jena, Germany) equipped with x-ray energy dispersive spectrometry (EDS) capabilities with an Oxford INCA energy 250 microanalysis system (Oxford

Instruments NanoAnalysis, MA, USA). Electrons were generated using a ZrO-W Schottky field emission gun source. All samples were mounted on aluminum stubs using carbon tape and they were coated with a 5 nm conductive film of gold using a sputter coater. The electron beam was set at 2.0 keV to prevent electron beam induced damage to the specimens and analyses were performed at different magnifications to obtain representative imaging data.

M3. Impact of of A:At treated recovered cellulose lyophilization on cellulase activity

A:At treated cellulose I and cellulose III generated after treatment for varying treatment durations were lyophilized for XRD analysis. Therefore, we also performed enzymatic hydrolysis on all lyophilized cellulose samples at a fixed enzyme loading (5 mg Cellic C.Tec2/g glucan) to study impact of lyophilization on cellulase activity. Briefly, all lyophilized pretreated cellulose samples were subjected to enzymatic hydrolysis at 2.5% glucan loading in 10 ml reaction volume using 15 ml glass vials as described before,[1] based on the original NREL protocols.[4] In all assays, final reaction volume pH 4.8 was achieved using 50 mM sodium citrate buffer and sodium azide was added to prevent any microbial growth (0.1% w/v final concentration). Vials were incubated at 50 °C in an orbital shaking incubator set at 150 RPM (New Brunswick, Innova 44, Enfield, CT) for desired saccharification time (24, 72 h). The hydrolysate supernatants were analyzed for total reducing sugar concentrations using the standard dinitrosalicylic acid (DNS) colorimetric assay or glucose/xylose based enzymatic assay kits as reported earlier.[5]

M4. Corn stover A:At pretreatment mass balance and compositional analysis methods

The corn stover used here was generously provided by the Great Lakes Bioenergy Research Center (GLBRC). The moisture content of the milled corn stover was approximately 9% (total weight basis) and was used as is for A:At pretreatment without any pre-activation of the cellulose. Briefly, corn stover was pretreated directly using a ~27:73% (dry weight basis or dwb) ammonia-ammonium thiocyanate solution as described below. A:At solution was prepared as described previously.[6,7] For all ex-situ ammonia-salt pretreatments, add 4 g (twb) of corn stover along with ~100 ml of ammonia-salt solution in a 500 mL stoppered glass bottle and mix slurry using a magnetic stirrer at 500 rpm for desired pretreatment time (24 h) at room temperature. At the desired sampling time after 24 h, add 100 mL of ethanol (100%) as anti-solvent to precipitate solubilized polysaccharides out of solution. Filter and wash the recovered solid precipitate with excess ethanol (50:1, v/w), followed by five washes with 1:1 ethanol-acetone (20:1, v/w) to remove any traces of residual ammonia-salt. Store all treated biomass samples in a never-dried state, soaked in 100% ethanol, at 4 °C prior to usage.

Untreated CS and A:At treated CS solids were subjected to compositional analysis using a slightly modified NREL/TP-510-42618 and NREL/TP-510-42620 protocols, where biomass was not extracted with water/ethanol prior to acid hydrolysis and neutralized sugar hydrolysates were analyzed using a suitable glucose/xylose enzyme assay kits to estimate sugar concentrations instead.[5] Mass balances on total glucan, xylan, and lignin (acid soluble and acid insoluble) were performed before and after the A:At pretreatment. Untreated corn stover contained approximately 40.6±0.8% glucan, 22.4±2.9% xylan, 21.5±2.9% Klason lignin, and 1.4±0.9% acid-soluble lignin based on a dry weight basis. While, A:At treated corn stover contained approximately 48.6±7.5% glucan, 23.5±0.0% xylan, 3.6±1.9% Klason lignin, and 1.2±0.4% acid-soluble lignin based on a dry weight basis. Here, all mass balance and compositional analysis experiments were done in two replicate batches conducted on two separate days each and the relevant mean values and

corresponding standard deviations are reported here. The A:At CS extractives composition was indirectly estimated based on the untreated CS and A:At CS substrate composition as well as the ~85% solids mass recovery values.

Please note that since we are currently interested in showing proof-of-concept of how an A:At type pretreatment process would actually work on real-world relevant lignocellulosic biomass, we monitored the changes in composition of corn stover for key representative monocot grasses cell wall components, namely cellulose, xylan, and acid-insoluble (Klason)/acid-soluble lignin. We did not attempt to perform a detailed composition analysis of all expected plant cell wall components, therefore the mass balance currently only accounts for ~77-85% of total dry weight of starting biomass material. The remaining 15-23% of the starting material will likely have significant contributions from arabinan (~3-5%), mannan (~1-2%), galactans (~2-3%), proteins (~3-5%), acetyls (~3-5%), uronic acids (~3-5%), and/or non-structural components like sucrose (~1-2%) and ash often reported in monocot grasses like stover. Templeton and co-workers have performed detailed analysis of different compositional analysis methods and systematically studied the overall variance in corn stover composition,[8,9] providing details on other likely cell wall components not analyzed currently. Future work will focus on investigating the detailed composition of corn stover as a function of various A:At pretreatment conditions at larger scale for increased mass balance accuracy and also identify the chemical/structural changes likely taking place during pretreatment analogous to work reported for AFEX/EA pretreatment.[10–12]

M5. Molecular dynamics simulations of model cellulose chain in A:At solvent system

Atomistic Model. The model cellulose chain used for all MD simulations was cellohexaose, which contains six β1-4 linked β-D-glucose monomers. Two solvent environments of cellohexaose were examined: 1) cellohexaose:ammonia:ammonium thiocyanate (A:At) with a relative weight ratio of 1.2:27:73, respectively; and 2) cellohexaose in water. The molecules were packed in a cubic box with a side length of 51 Å using Packmol.[13] To ensure our findings do not depend on one initial configuration, we performed three independent simulations (i.e., instances) with different initial structures and initial velocity distributions.

Force Field. CHARMM36 force field parameters were used for cellohexaose and ammonia,[14,15] and the TIP3P model[16] was used for water. For ammonium cation (NH_4^+), its force field parameters were derived from methylammonium ($CH_3NH_3^+$) in CHARMM,[14,15,17] and are shown in Table S2. For thiocyanate anion (SCN^-), we obtained its force field parameters using Force Field Toolkit (ffTK)[18] implemented in VMD[19] in combination with Gaussian09.[20] We then optimized its Lennard-Jones potential until the simulation-derived solvation free energy (ΔG_{sol}) was in good agreement with experiment.[21] Table S3 shows the optimized force field parameters for SCN^- employed in this work. To validate the parameters for NH_4^+ and SCN^-, we calculated their ΔG_{sol} from the MD simulations and compared them to experiment (Table S4).

MD Simulations. We employed the GROMACS simulation code.[22] For each of the three instances, we first performed energy minimization followed by 5 ns of equilibration and 110 ns of production in an NPT ensemble with a time step of 1 fs at 293 K and 0.55 bar to model the vapor pressure of ammonia in a closed container.[23] 300 K and 1 bar were applied to cellohexaose in water. We used a v-rescale thermostat[24] with 0.1 ps as the time constant for coupling to maintain constant temperature, and Berendsen[25] and Parrinello-Rahman[26] barostats with 1 ps as the time constant for

coupling to maintain constant pressure for equilibration and production, respectively. The isothermal compressibility for pressure coupling was 0.00015 bar^{-1}, which applies to liquid ammonia at 293 K.[27] We used Verlet cutoff-scheme, fast smooth particlemesh Ewald (PME)[28] electrostatics and linear constraint solver (LINCS)[29] algorithm on hydrogen-containing bonds. The instantaneous energies and configurations were saved every 10 ps. The last 100 ns for each of the three instances were used for analysis, and all the calculated values represent averages over the three instances. Figure S5 shows a snapshot of the equilibrated cellohexaose in A:At solvent. Movie S1 shows how the structure of cellohexaose changes in A:At solvent along MD simulation time and can be downloaded on the RSC website.

Conformations of the C6-Hydroxymethyl Group. We examined the conformations of the C6-hydroxymethyl group of cellohexaose in A:At and in water, excluding the two glucose monomers at chain ends. We analyzed the probability distribution of the dihedral angle ϕ of O5-C5-C6-O6 (Figure S6). ϕ = -60°, 60°, and -180° correspond to Gauche-Gauche (GG), Gauche-Trans (GT), and Trans-Gauche (TG) conformations.[30] We also obtained the relative populations of these conformations by calculating the area under each peak. The relative populations of GG:GT:TG in A:At and water are 0.35:0.48:0.17 and 0.47:0.45:0.08, respectively. Our results show that GG and GT conformations dominate in water, in agreement with a previous study.[30] Compared to water, there is a larger GG population and a smaller GT in A:At.

Cellohexaose - A:At Interactions. We resolved molecular interactions of cellohexaose with A:At solvent by calculating the radial distribution function g(r), a measure of local concentration of target species as a function of distance r from reference species,[31] between cellulose oxygen atoms that participate in the intra-chain hydrogen bonding in cellulose crystal structure.[32] Figures S7-S9 show that O2, O6, and O3 atoms interact much more strongly with ammonium cations, evidenced by the height of the first peak, as compared with thiocyanate anions and ammonia. In Figure S10, the interactions between O5 atoms and ammonium cations at r ~ 2.9 Å are still stronger than thiocyanate anions and ammonia, but its strength g(r) is much less than the other oxygen atoms in cellohexaose (Figure S11). This is likely to be attributed to the hydrogen bonding between O5 and O3 atoms.

Hydrogen Bonding Analysis. Table S5 shows that the hydrogen bonding between O2, O6, and O3 hydroxyl groups and nitrogen atoms of ammonium cations is significantly greater than thiocyanate cations and ammonia, and that O5 atoms have much weaker hydrogen bonding with ammonium cations as compared with other oxygen atoms. These hydrogen-bond findings are consistent with the g(r) results. We also see that 98% of the intra-chain O2-O6 hydrogen bonding is disrupted in A:At solvent, while only 43% of O3-O5 hydrogen bonding is disrupted. Since O3-O5 is not mostly disrupted in A:At solvent, the cellohexaose is unlikely to fold on itself and form globular shapes. A modification in formulation of A:At solvent may be required in future work to achieve globular cellulose chains as published in a recent study that used dimethyl sulfoxide to assist with cellulose dissolution in 1-ethyl-3-methylimidazoium acetate.[33]

A:At Solvent Interactions. Figure S12 shows that the interaction between ammonium cations (NH_4^+) and ammonia (NH_3) is much stronger than the other two solvent-solvent pairs. This suggests that NH_4^+-NH_3 clusters may occur in A:At solvent, which agrees with our hypothesis in experiment.

M6. Comment on viscosity of A:At and cellulose-A:At based solvent systems

Previous work has shown than ammonia based pretreatments like AFEX or EA do not significantly change cellulose degree of polymerization (DP) since cellulose polymer chain glycosidic bonds are mostly stable under AFEX-like treatment conditions at temperatures between 90-130 °C.[34] Other alkaline-catalyzed (i.e., NaOH based) cleavage reactions of cellulose glycosidic linkages to reduce cellulose DP are also virtually non-existent at room temperature.[35] This is largely because base-catalyzed cleavage of glycosidic bonds is highly sensitive to temperature. This is further clear when comparing kinetic data of the peeling-off reactions with those of alkaline hydrolysis reactions, it is obvious that alkaline hydrolysis of glycosidic bonds is a relatively slow process even at higher temperatures.[36,37] For example, Sarkanen and co-workers determined that at room temperature (25 °C), the rate constant of glycosidic bond cleavage is about 7 orders of magnitude lower than the rate observed at temperatures exceeding 150 °C.[35] Even though such reactions only become relevant during alkaline pulping or ammonia-based treatments of cellulose at temperatures exceeding 150 °C, the extent of glycosidic bond cleavage even under these extreme conditions can be marginal compared to acid-catalyzed glycosidic bond cleavage reactions. Furthermore, even any cellulose degradation which is mostly driven by reducing-end specific secondary peeling-off type reactions that do not change cellulose DP significantly since these reactions that could reduce DP are often terminated by competing stopping-type reactions. Lastly, considering that ammonia is also a weaker alkali than sodium hydroxide, it is expected that cellulose DP will also not change significantly during anhydrous ammonia-based treatments at temperatures close to 25 °C. Similarly at room temperature/pressure, A:At type solvents have also been shown to not alter cellulose DP based on the near-constant viscosity observed for cellulose-A:At solutions at 25 °C.[7] Hudson and Cuculo (1980) showed that no degradation in cellulose DP can be inferred based on the near constant viscosity of the cellulose-A:At solution at room temperature even after 24 hours. A ^{13}C-NMR study further validated that no cleavage of the glycosidic bonds was seen to take place for cellulose in the A:At solvent system.[38]

Therefore, since there was no significant change in cellulose DP or solution viscosity reported by Cuculo and co-workers for cellulose-A:At solution once the cellulose is fully dissolved in the A:At solvent, we did not attempt to monitor the viscosity change of our A:At-cellulose solutions once cellulose was full dissolved. Hudson and Cuculo (1983) also showed that the kinematic viscosity of typical A:At solutions ranged between 2-5 centistokes (cSt) at temperatures ranging between 15-35 °C at zero shear rate.[7,39] The kinematic viscosity of A:At solution alone of comparable composition, to what was reported in our current study, at 25 °C is ~3 centistokes at zero shear rate. Based on these published reports, the dynamic viscosity of equivalent A:At solution alone is therefore expected to be around 0.003 Pascal second (i.e., assuming A:At solvent density ~0.99 g/ml at 25 °C). For cellulose-A:At solutions (at ~0.02-0.2 wt% cellulose concentration), Cuculo and co-workers (Hudson 1980 and Hudson 1983) determined the relative viscosity of cellulose-A:At solutions with respect to the solvent alone at 25 °C to range between 1.2-2 for low DP cellulose samples most closely equivalent to Avicel used in our study.[7,39] We expect a similar fold change increase in the relative viscosity of the cellulose-A:At solutions once either cellulose I or III allomorphs is fully dissolved into solution. Since the concentration of cellulose used in our *ex-situ*/*in-situ* pretreatment studies were slightly higher (~2-to-5 w/v% cellulose in A:At solution), we expect the fold-change in relative viscosity to be greater than 2-fold once cellulose is fully dissolved in solution. Future work is needed to explore if there is any difference in viscosity of cellulose-A:At solutions for cellulose I versus III, though unlikely, once the cellulose is fully

dissolved in solution in either case. However, based on the SANS analysis (Table 2), cellulose III and cellulose I dissolved in A:At solution after 4 h and 72 h, respectively, have comparable structural properties. This suggests that once cellulose is fully dissolved into A:At solution the starting cellulose allomorph type will likely have limited effect, if at all any difference, on the final cellulose solution viscosity.

Furthermore, please note that the dynamic viscosity of the A:At solution alone and equivalent concentration cellulose-A:At solution is nearly 2-3 orders of magnitude lower than the viscosity of commonly reported ionic liquids (IL; e.g., 1-ethyl-3-methylimidazolium acetate) and relevant cellulose-IL solutions under comparable dissolution conditions (e.g., dissolution temperature, cellulose concentration) and cellulose properties (e.g., cellulose DP and initial crystallinity).[40] This highlights that A:At is a better low viscosity solvent for cellulose dissolution at room temperature compared to conventional ILs like 1-ethyl-3-methylimidazolium acetate that have been reported for cellulose pretreatment at process relevant biomass loading conditions.

ESI Tables and Figures:

Table S1. XRD crystallinity index (using Segal Method) and cellulose 002 equatorial reflection deconvoluted peak crystallite size (using Scherrer Method) for Avicel PH-101 cellulose-I, cellulose-III (CIII; bottom), and corresponding A:At treated samples is tabulated here. All A:At sample treatment time is provided on sample type labels along with identifier C1 (cellulose I) or C3 (cellulose III) to indicated source of starting material used for A:At treatment. All A:At treated samples were lyophilized prior to XRD analysis and data was analyzed as discussed in the ESI methods section. Note that the non-lyophilized samples were used to conduct enzymatic hydrolysis at 0.5 mg C. Tec2 enzyme/g glucan loading for 24 h saccharification time period and the hydrolysis results as a function of cellulose crystallite size reported in table below were also plotted as seen in Figure 2A.

Sample Type	%CrI (Segal)	Crystallite size (nm)
C3 control	79	4.2
AAt-C3-1 h	49	2.0
AAt-C3-3 h	48	1.9
AAt-C3-6 h	40	1.5
AAt-C3-24 h	53	1.7
Sample Type	**%CrI (Segal)**	**Crystallite size (nm)**
C1 control	84	5.1
AAt-C1-1 h	80	4.9
AAt-C1-3 h	80	5.1
AAt-C1-6 h	80	4.8
AAt-C1-24 h	79	4.3

Table S2. Force field parameters for NH_4^+ used in this work. The notations follow the convention of CHARMM,[17] and L-J stands for Lennard-Jones.

Species		Parameter	Value
N	charge	q [C]	-0.32
	L-J	ε [kcal/mol]	-0.20
		$R_{min}/2$ [Å]	1.85
H	charge	q [C]	0.33
	L-J	ε [kcal/mol]	-0.046
		$R_{min}/2$ [Å]	0.225
N-H	bonds	K_b [kcal/mol/Å^2]	403.00
		b_0 [Å]	1.04
H-N-H	angles	K_θ [kcal/mol/rad^2]	44.00
		θ_0 [deg]	109.50

Table S3. Force field parameters for SCN^- used in this work. The notations follow the convention of CHARMM,[17] and L-J stands for Lennard-Jones.

Species		Parameter	Value
S	charge	q [C]	-0.876
	L-J	ε [kcal/mol]	-0.35
		$R_{min}/2$ [Å]	2.75
C	charge	q [C]	0.071
	L-J	ε [kcal/mol]	-0.18
		$R_{min}/2$ [Å]	1.87
N	charge	q [C]	-0.195
	L-J	ε [kcal/mol]	-0.18
		$R_{min}/2$ [Å]	1.79
S-C	bonds	K_b [kcal/mol/Å^2]	314.639
		b_0 [Å]	1.666
C-N	bonds	K_b [kcal/mol/Å^2]	922.829
		b_0 [Å]	1.198
S-C-N	angles	K_θ [kcal/mol/rad^2]	3.316
		θ_0 [deg]	179.990

Table S4. Comparison between MD simulations and experiments for ΔG_{sol} [kJ/mol] of NH_4^+ and SCN^-. ΔG_{sol} was calculated following the procedures published previously.[31]

Component	MD simulations	Experiment[21]	Error
NH_4^+	-289.59 ± 0.06	-285	2%
SCN^-	-290.98 ± 0.23	-280	4%

Table S5. Hydrogen bonding analysis on cellohexaose-A:At solvent and intra-cellohexaose in A:At solvent and crystal structure. Donors are OH or NH groups, and acceptors are nitrogen or oxygen atoms. A^+, T^-, and A correspond to ammonium cation, thiocyanate anion, and ammonia, respectively. The disruption % is the difference in hydrogen bond number between crystal structure and A:At solvent divided by the number in crystal structure.

Donor-Acceptor	Hydrogen bond # in A:At solvent	Hydrogen bond # in crystal structure	Disruption % in A:At solvent
O2-NA^+	2.013 ± 0.006		
O2-NT^-	0.687 ± 0.004		
O2-NA	1.030 ± 0.006		
O6-NA^+	2.947 ± 0.006		
O6-NT^-	0.572 ± 0.004		
O6-NA	1.020 ± 0.006		
O3-NA^+	2.620 ± 0.007		
O3-NT^-	0.272 ± 0.003		
O3-NA	0.957 ± 0.005		
NA^+-O5	0.143 ± 0.002		
NA-O5	0.252 ± 0.003		
O3-O5	2.855 ± 0.006	5	43
O2-O6	0.083 ± 0.002	5	98
O6-O2	0.485 ± 0.004		

Figure S1. Representative SEM images of controls and 24 h A:At treated cellulose samples at 3000X and 500X magnifications. All samples were lyophilized prior to SEM imaging.

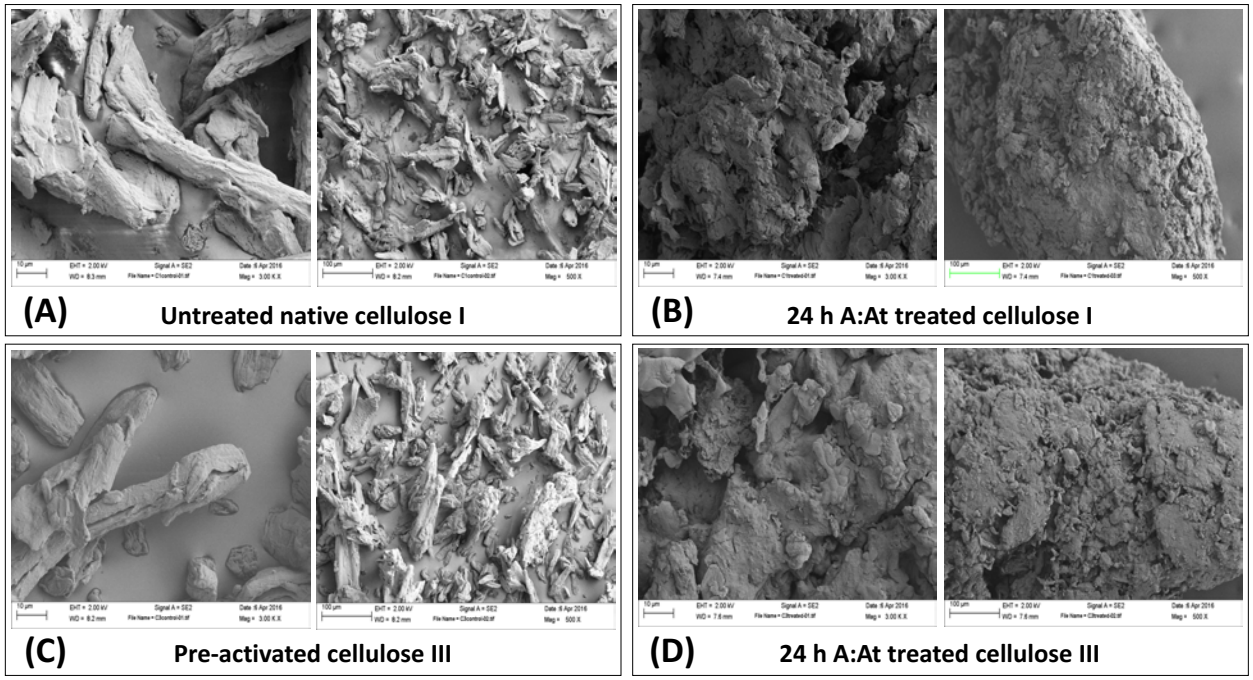

Figure S2. Representative XRD raw data (in blue) and corresponding peak deconvolution fitted spectra (in yellow) for Avicel PH-101 cellulose-I (CI; top) and cellulose-III (CIII; bottom) controls is shown here. The deconvoluted gaussian peaks for each fitted XRD spectra is shown immediately below in each XRD plot. Note that y-axis units here are XRD spectra intensity counts while x-axis units are the 2θ Bragg's scattering angle.

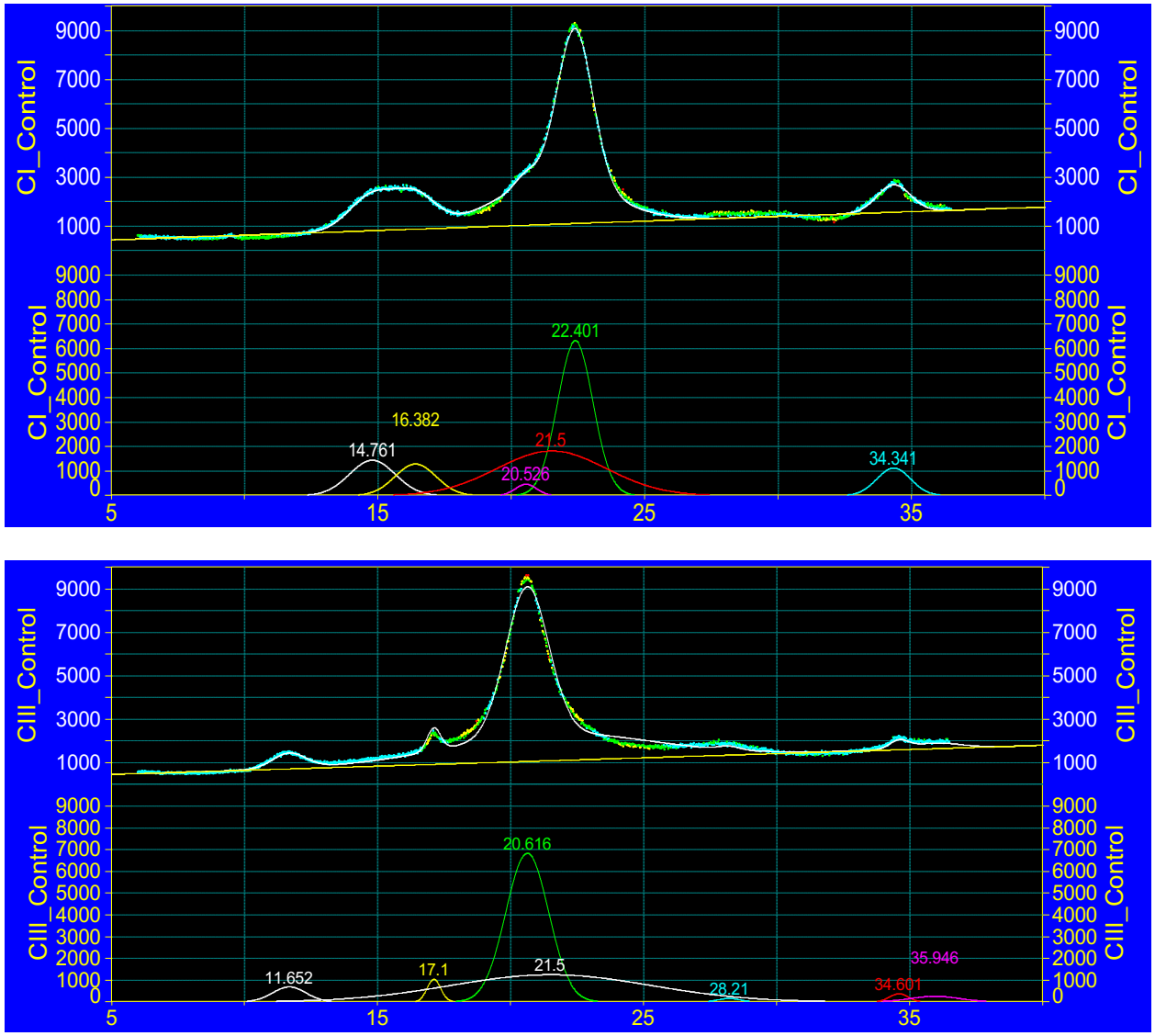

Figure S3. Impact of A:At pretreated cellulose lyophilization on enzymatic hydrolysis conversion yields, after 24 and 72 h, obtained for both controls (cellulose I or cellulose III) and respective A:At treated cellulose samples. All A:At sample treatment time is provided on the x-axis labels along with identifier CI (cellulose I) or CIII (cellulose III) to indicated source of starting material used for A:At treatment. All A:At treated samples were lyophilized prior to saccharification.

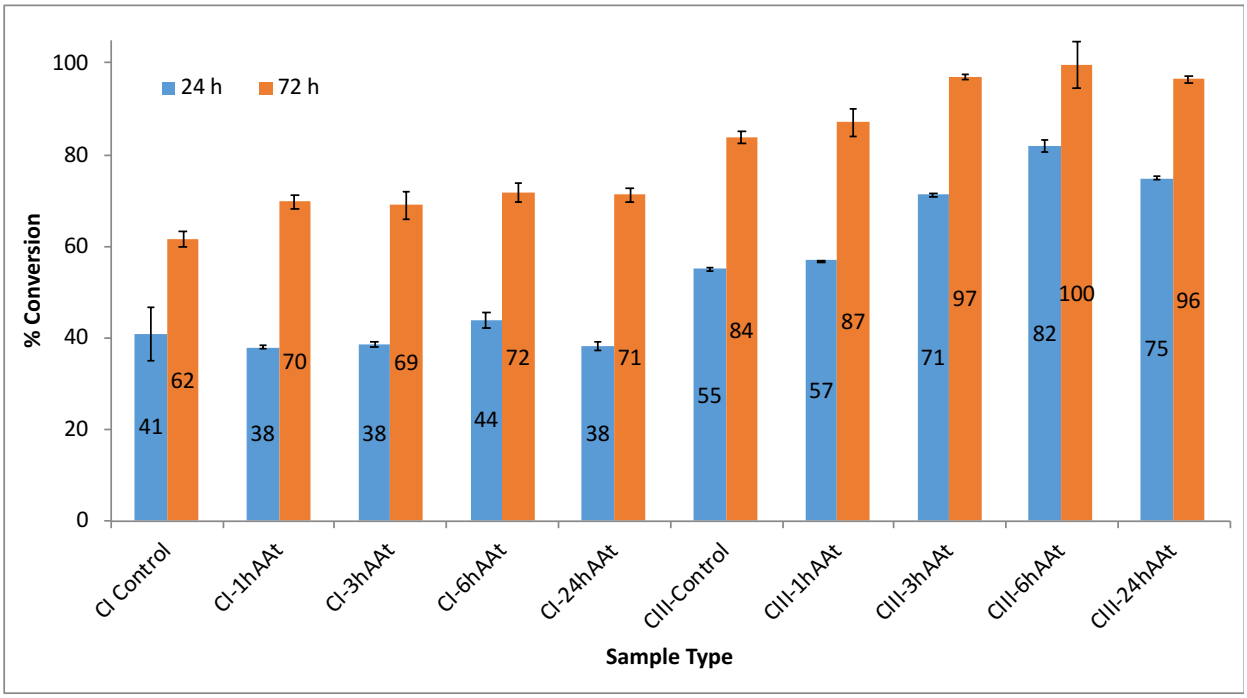

Figure S4. Small-angle neutron scattering (SANS) plot profiles for replicate sample runs are highly reproducible, as illustrated below. Here, S1 (in red below) vs. S2 (in blue above) are replicate 24 h ex-situ A:At treated cellulose III samples recovered and suspended in D_2O prior to SANS analysis.

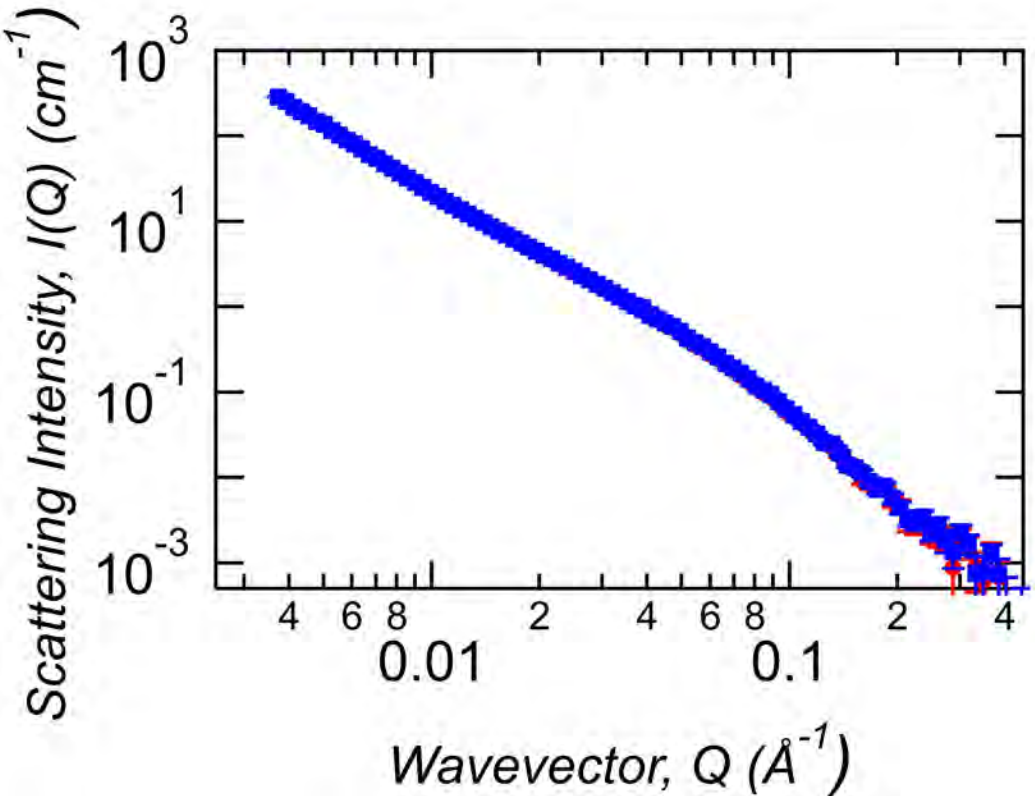

Figure S5. Equilibrated cellohexaose atomistic configurations in A:At solvent within 5 Å of cellohexaose at 293 K and 0.55 bar. Cellohexaose is shown in green, ammonia and ammonium cations are shown in blue, and thiocyanate anions are shown in magenta.

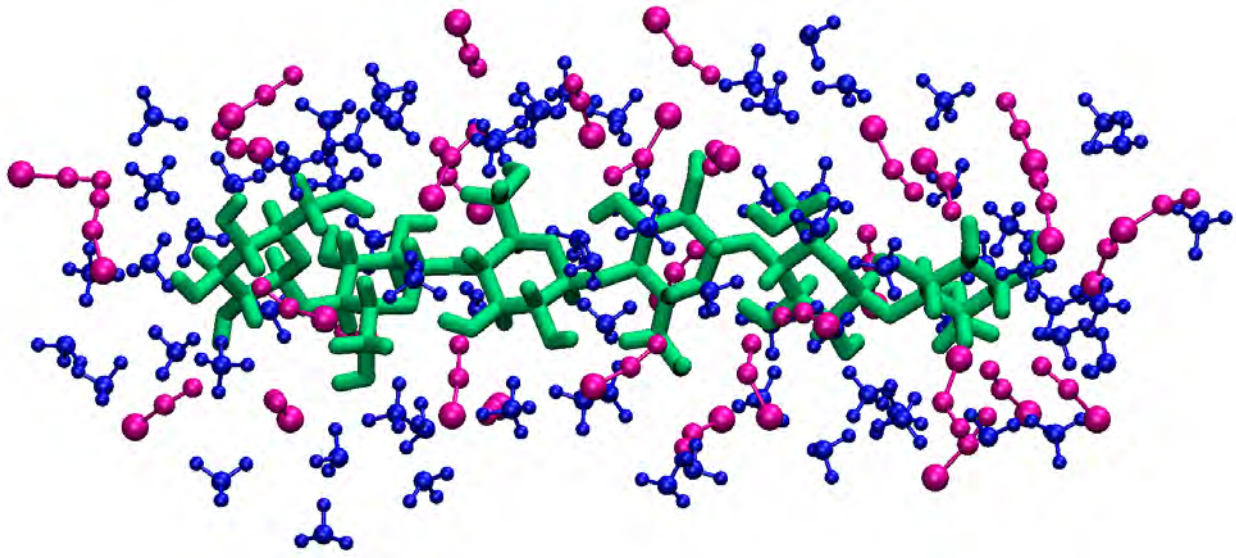

Figure S6. Probability distribution P(ϕ) with standard error bars of the dihedral angle ϕ of O5-C5-C6-O6, which determines the conformation (GG, GT, or TG) of the C6-hydroxymethyl groups, for cellohexaose in A:At or water.

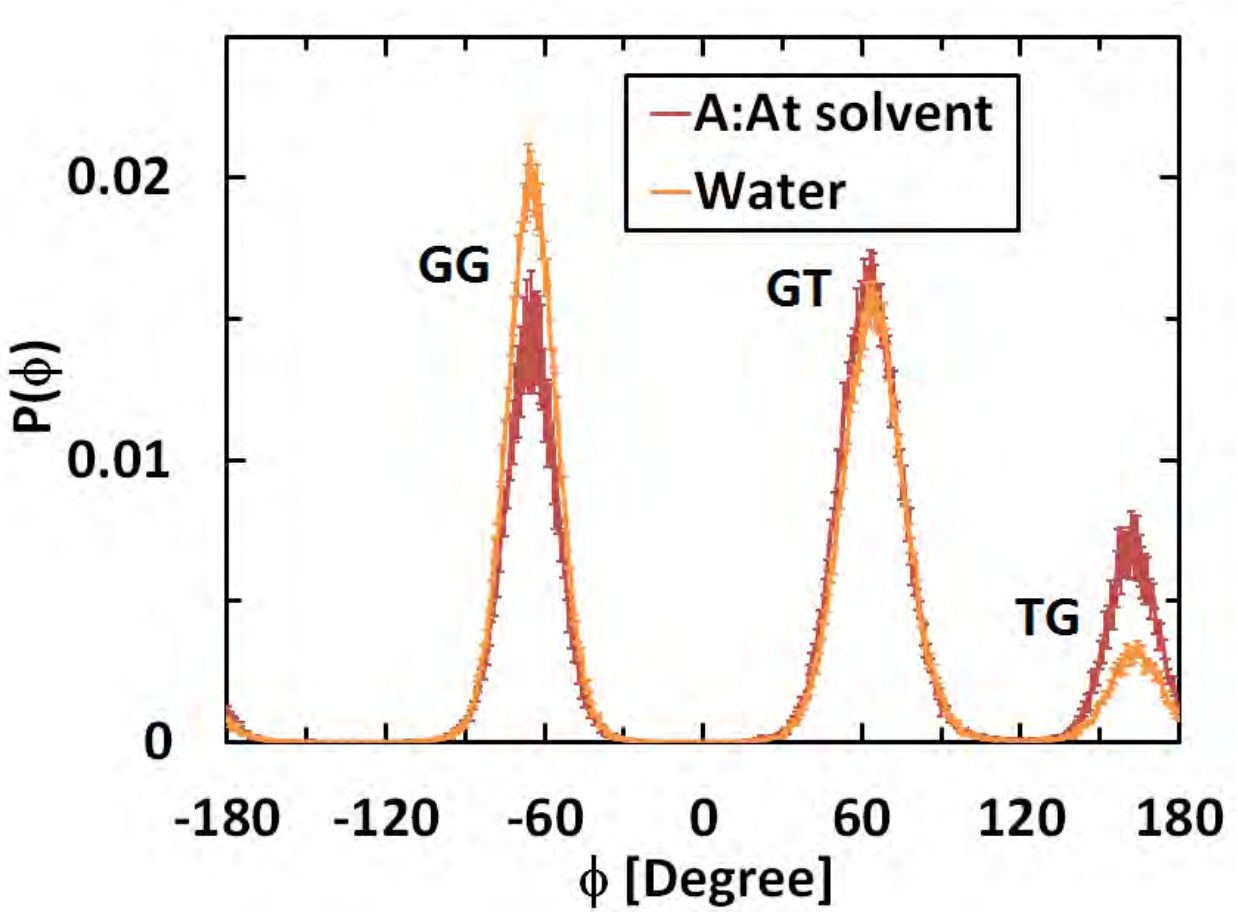

Figure S7. Radial distribution function g(r) between O2 atoms (reference) of cellohexaose and N atoms (target) of A:At solvent with standard error bars. A^+ is ammonium cation, T^- is thiocyanate anion, and A is ammonia.

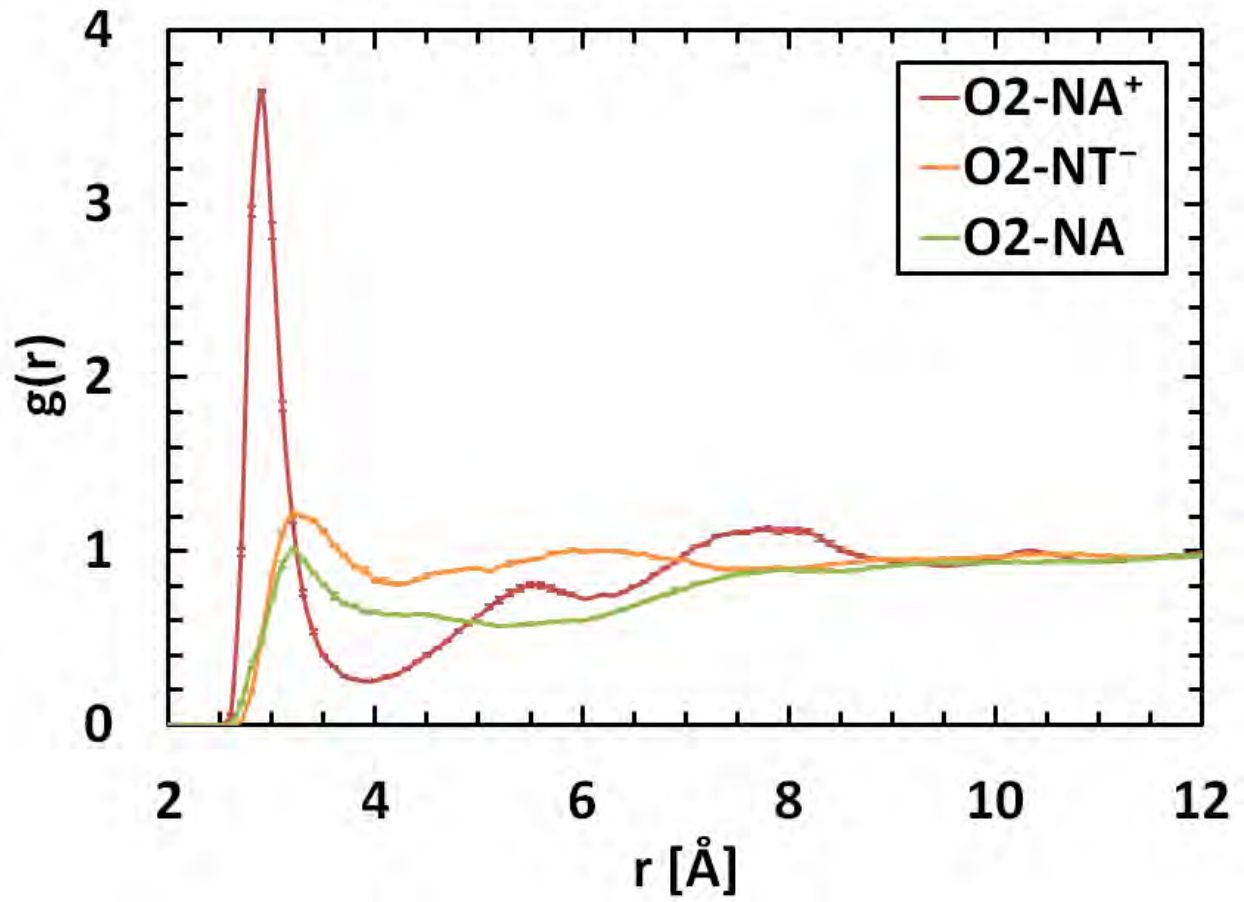

Figure S8. Radial distribution function g(r) between O6 atoms (reference) of cellohexaose and N atoms (target) of A:At solvent with standard error bars. A^+ is ammonium cation, T^- is thiocyanate anion, and A is ammonia.

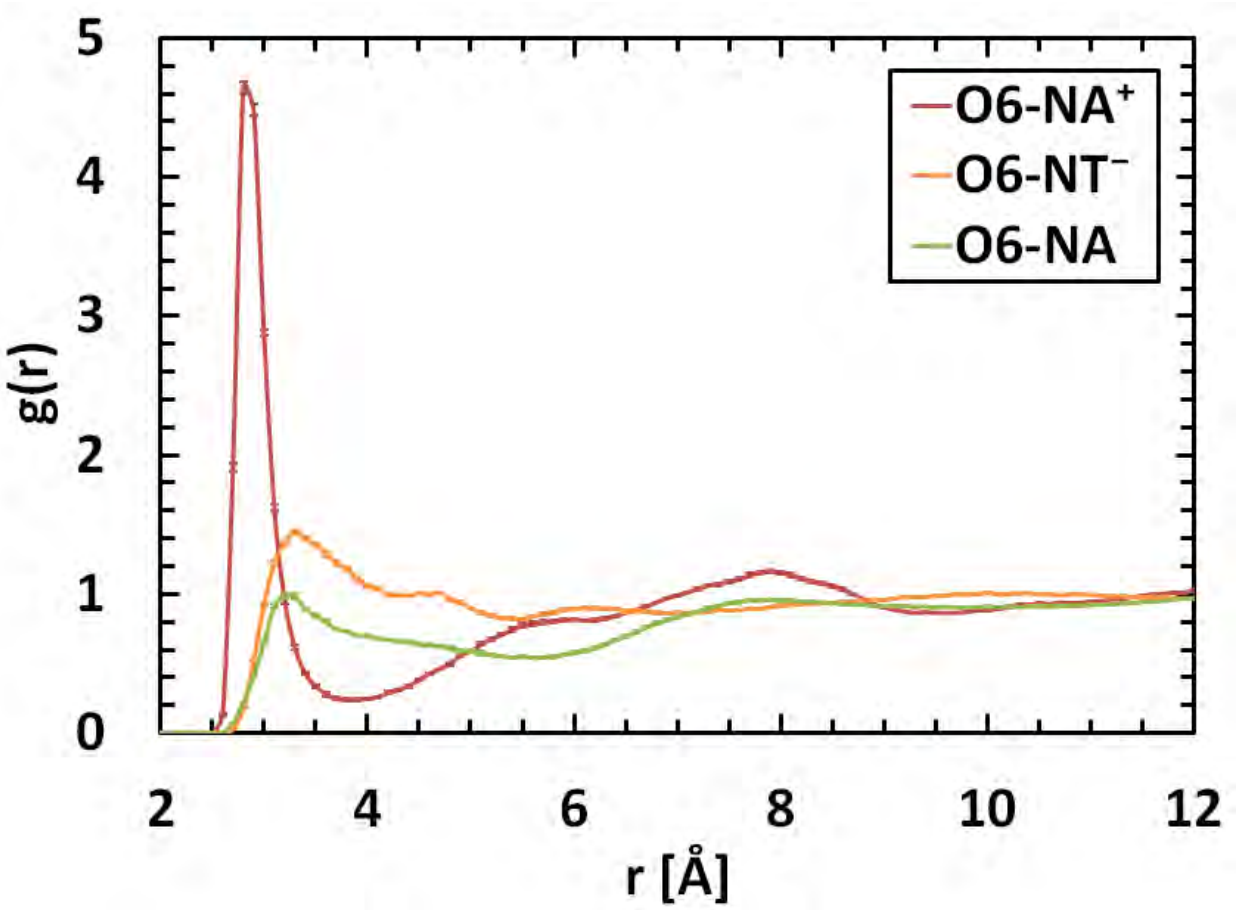

Figure S9. Radial distribution function g(r) between O3 atoms (reference) of cellohexaose and N atoms (target) of A:At solvent with standard error bars. A^+ is ammonium cation, T^- is thiocyanate anion, and A is ammonia.

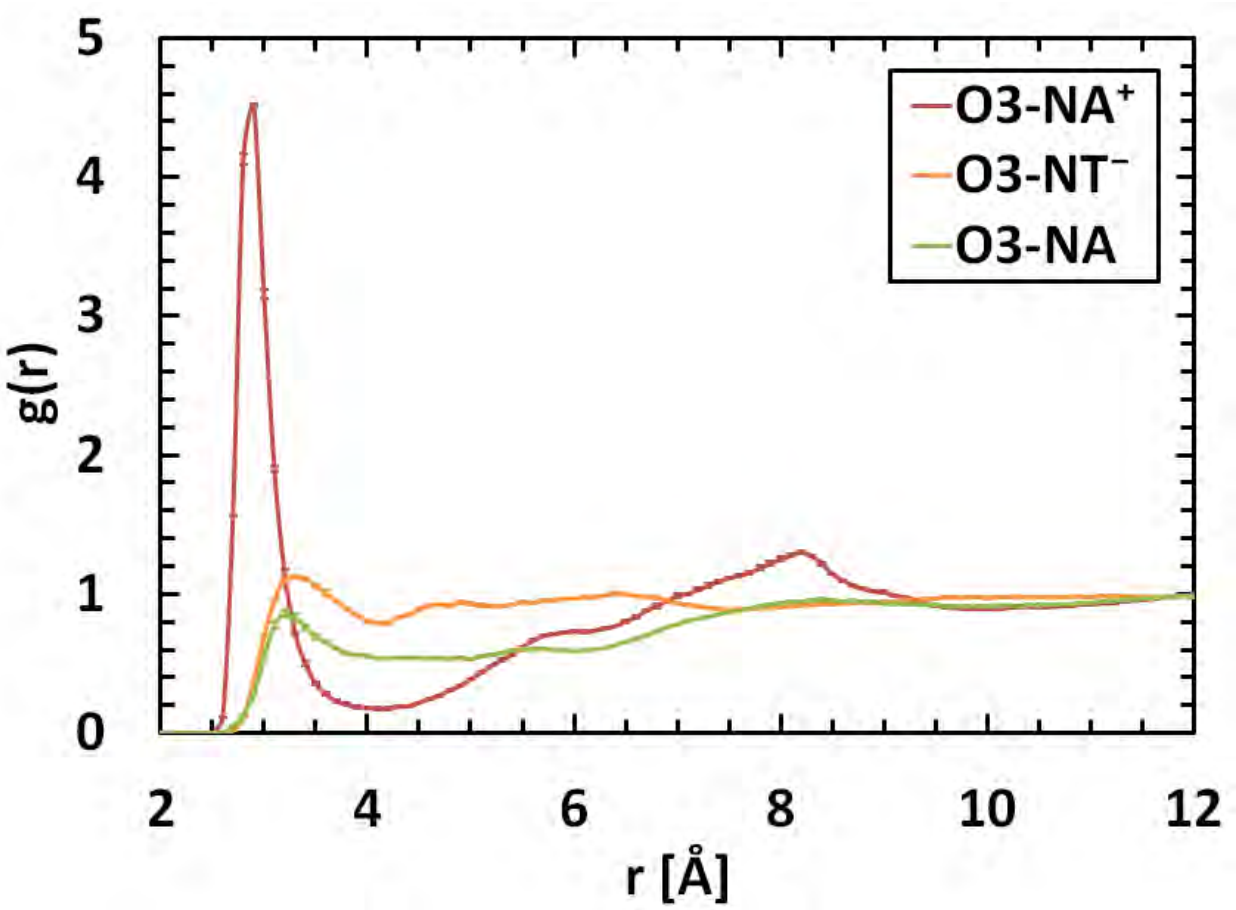

Figure S10. Radial distribution function g(r) between O5 atoms (reference) of cellohexaose and N atoms (target) of A:At solvent with standard error bars. A^+ is ammonium cation, T^- is thiocyanate anion, and A is ammonia.

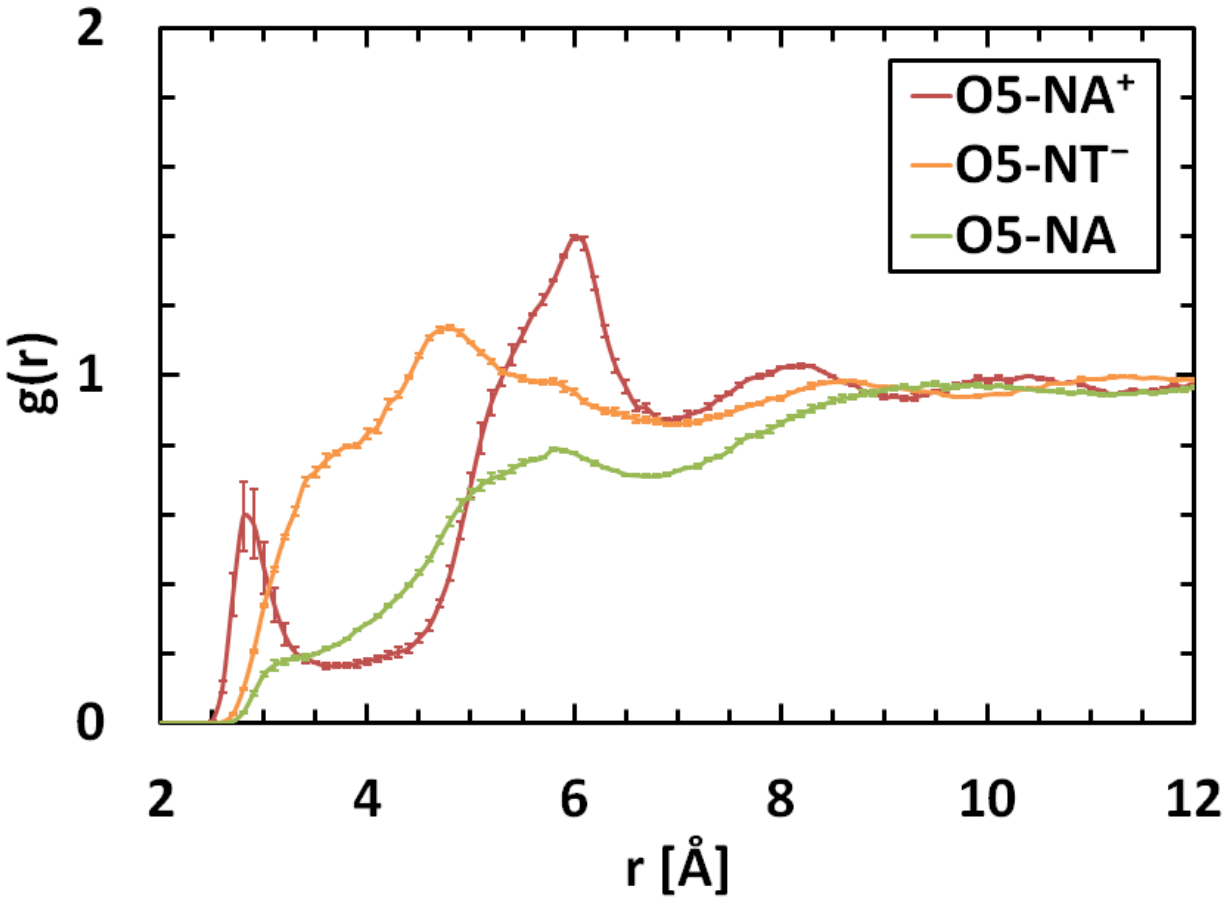

Figure S11. Radial distribution function g(r) between O atoms (reference) of cellohexaose and N atoms (target) of ammonium cation (A^+) with standard error bars.

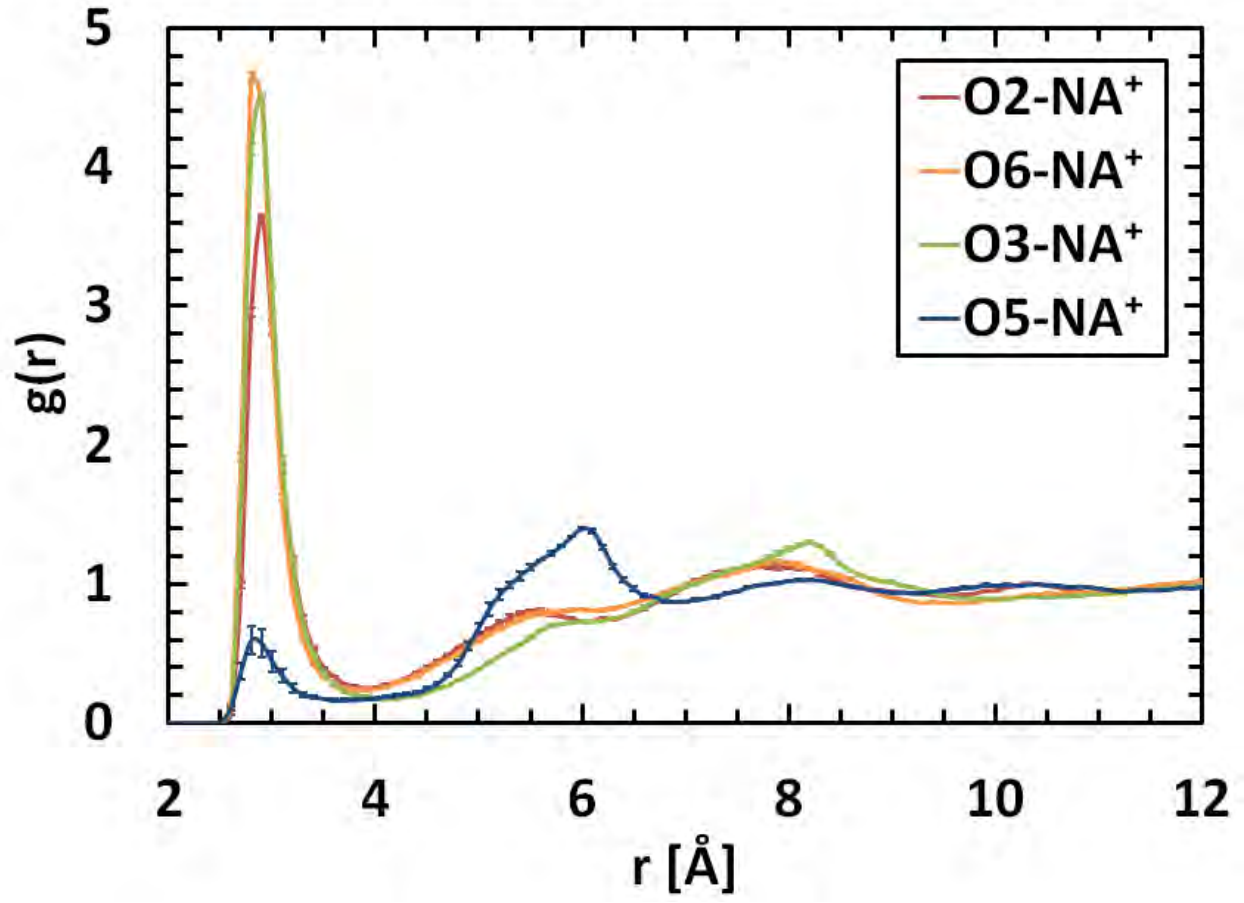

Figure S12. Radial distribution function g(r) between nitrogen atoms of each solvent-solvent pair with standard error bars. A^+ is ammonium cation, T^- is thiocyanate anion, and A is ammonia.

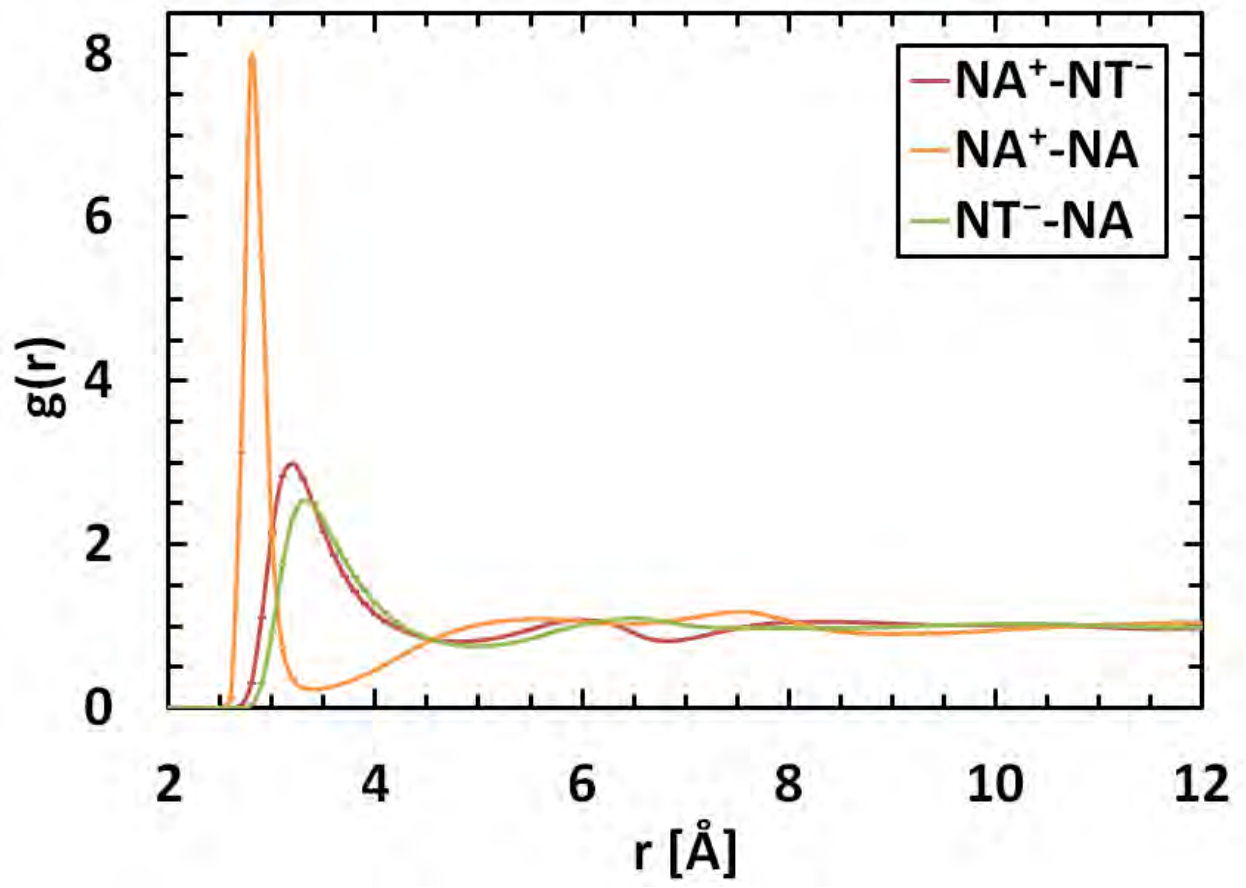

Figure S13. Impact of A:At pretreatment time (3, 6, or 24 h) on enzymatic saccharification rate, obtained for both controls (cellulose III or cellulose I) and respective A:At treated cellulose samples, at various C. Tec2 cellulase enzyme loadings ranging from 0.05-5 mg enzyme/g glucan loading. Here, (A) shows data for cellulose III while (B) shows cellulose I relevant data. All hydrolysis reactions were conducted for 24 hours and total solubilized sugar concentration in the supernatant were then quantified using standard DNS assay (using glucose as standard).

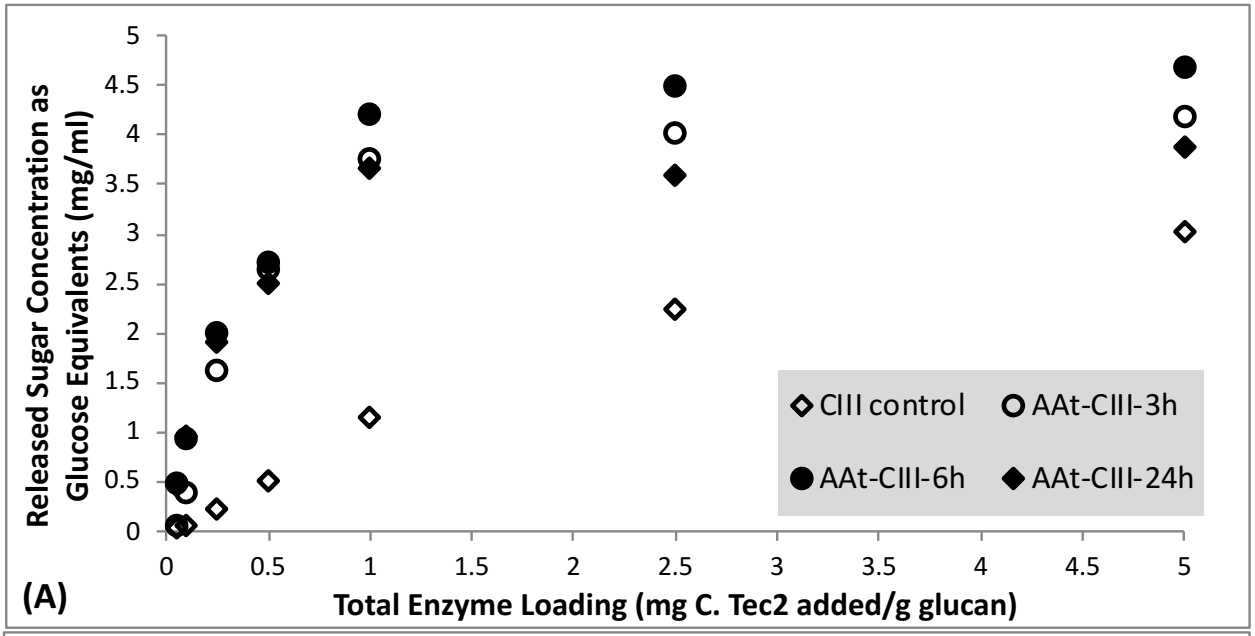

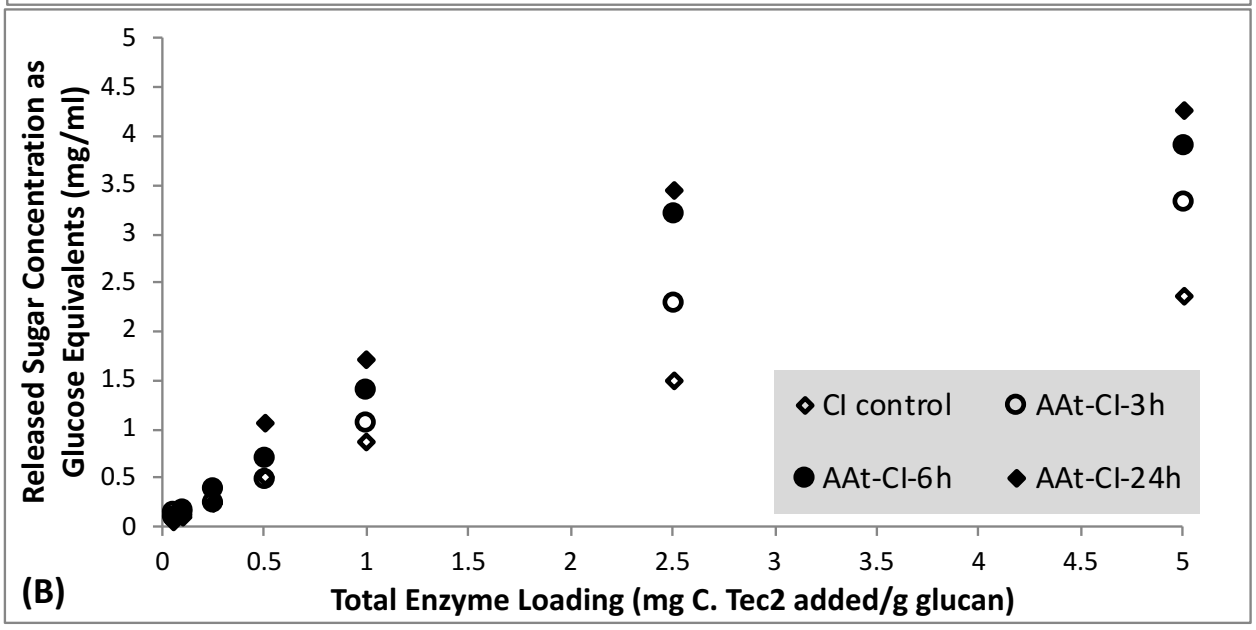

ESI Additional References

(1) Chundawat, S. P. S.; Bellesia, G.; Uppugundla, N.; Sousa, L.; Gao, D.; Cheh, A.; Agarwal, U.; Bianchetti, C.; Phillips, G.; Langan, P.; Balan, V.; Gnanakaran, S.; Dale, B. E. Restructuring the Crystalline Cellulose Hydrogen Bond Network Enhances Its Depolymerization Rate. *J. Am. Chem. Soc.* **2011**, *133* (29), 11163–11174 DOI: 10.1021/ja2011115.

(2) Park, S.; Baker, J.; Himmel, M.; Parilla, P.; Johnson, D. Cellulose Crystallinity Index: Measurement Techniques and Their Impact on Interpreting Cellulase Performance. *Biotechnol. Biofuels* **2010**, *3* (1), 10.

(3) Garvey, C. J.; Parker, I. H.; Simon, G. P. On the Interpretation of X-Ray Diffraction Powder Patterns in Terms of the Nanostructure of Cellulose I Fibres. *Macromol. Chem. Phys.* **2005**, *206* (15), 1568–1575 DOI: 10.1002/macp.200500008.

(4) Resch, M. G.; Baker, J. O.; Decker, S. R. Low Solids Enzymatic Saccharification of Lignocellulosic Biomass. *Tech. Rep. NREL/TP-5100-63351, Lab. Anal. Proced.* **2015**, No. February, 1–9 DOI: 10.1016/j.jallcom.2018.03.019.

(5) Gao, D.; Chundawat, S. P. S.; Krishnan, C.; Balan, V.; Dale, B. E. Mixture Optimization of Six Core Glycosyl Hydrolases for Maximizing Saccharification of Ammonia Fiber Expansion (AFEX) Pretreated Corn Stover. *Bioresour. Technol.* **2010**, *101* (8), 2770–2781 DOI: 10.1016/j.biortech.2009.10.056.

(6) De Groot, A. W.; Guinnup, D. E.; Thiel, M. H.; Cuculo, J. A. Light-Scattering Studies on Solutions of Cellulose in the Ammonia / Ammonium Thiocyanate Solvent System. II. Quasielastic Light-Scattering and Liquid Crystal Study. *J. Polym. Sci. Part B Polym. Phys.* **1991**, *29* (5), 557–563 DOI: 10.1002/polb.1991.090290505.

(7) Hudson, S. M.; Cuculo, J. A. The Solubility of Cellulose in Liquid Ammonia/Salt Solutions. *J. Polym. Sci. Polym. Chem. Ed.* **1980**, *18* (12), 3469–3481 DOI: 10.1002/pol.1980.170181214.

(8) Sluiter, J. B.; Ruiz, R. O.; Scarlata, C. J.; Sluiter, A. D.; Templeton, D. W. Compositional Analysis of Lignocellulosic Feedstocks. 1. Review and Description of Methods. *J. Agric. Food Chem.* **2010**, *58* (16), 9043–9053 DOI: 10.1021/jf1008023.

(9) Templeton, D. W.; Scarlata, C. J.; Sluiter, J. B.; Wolfrum, E. J. Compositional Analysis of Lignocellulosic Feedstocks. 2. Method Uncertainties. *J. Agric. Food Chem.* **2010**, *58* (16), 9054–9062 DOI: 10.1021/jf100807b.

(10) da Costa Sousa, L.; Jin, M.; Chundawat, S. P. S.; Bokade, V.; Tang, X.; Azarpira, A.; Lu, F.; Avci, U.; Humpula, J.; Uppugundla, N.; Gunawan, C.; Pattathil, S.; Cheh, A. M.; Kothari, N.; Kumar, R.; Ralph, J.; Hahn, M. G.; Wyman, C. E.; Singh, S.; Simmons, B. A.; Dale, B. E.; Balan, V. Next-Generation Ammonia Pretreatment Enhances Cellulosic Biofuel Production. *Energy Environ. Sci.* **2016**, *9*, 1215–1223 DOI: 10.1039/C5EE03051J.

(11) da Costa Sousa, L.; Foston, M.; Bokade, V.; Azarpira, A.; Lu, F.; Ragauskas, A. J.; Ralph, J.; Dale, B.; Balan, V. Isolation and Characterization of New Lignin Streams Derived from Extractive-Ammonia (EA) Pretreatment. *Green Chem.* **2016**, *18* (15), 4205–4215 DOI:

10.1039/C6GC00298F.

(12) Chundawat, S. P. S.; Donohoe, B. S.; Sousa, L.; Elder, T.; Agarwal, U. P.; Lu, F.; Ralph, J.; Himmel, M. E.; Balan, V.; Dale, B. E. Multi-Scale Visualization and Characterization of Plant Cell Wall Deconstruction during Thermochemical Pretreatment. *Energy Environ. Sci.* **2011**, *4* (3), 973–984 DOI: 10.1039/C0EE00574F.

(13) Martínez, L.; Andrade, R.; Birgin, E. G.; Martínez, J. M. PACKMOL: A Package for Building Initial Configurations for Molecular Dynamics Simulations. *J. Comput. Chem.* **2009**, *30* (13), 2157–2164 DOI: 10.1002/jcc.21224.

(14) Yu, W.; He, X.; Vanommeslaeghe, K.; MacKerell, A. D. Extension of the CHARMM General Force Field to Sulfonyl-Containing Compounds and Its Utility in Biomolecular Simulations. *J. Comput. Chem.* **2012**, *33* (31), 2451–2468 DOI: 10.1002/jcc.23067.

(15) Vanommeslaeghe, K.; Hatcher, E.; Acharya, C.; Kundu, S.; Zhong, S.; Shim, J.; Darian, E.; Guvench, O.; Lopes, P.; Vorobyov, I.; Mackerell, A. D. CHARMM General Force Field: A Force Field for Drug-like Molecules Compatible with the CHARMM All-Atom Additive Biological Force Fields. *J. Comput. Chem.* **2009**, *31* (4), NA-NA DOI: 10.1002/jcc.21367.

(16) Jorgensen, W. L.; Chandrasekhar, J.; Madura, J. D.; Impey, R. W.; Klein, M. L. Comparison of Simple Potential Functions for Simulating Liquid Water. *J. Chem. Phys.* **1983**, *79* (2), 926–935 DOI: 10.1063/1.445869.

(17) D. MacKerell, A.; Bashford, D.; Bellott, M.; L. Dunbrack, R.; D. Evanseck, J.; J. Field, M.; Fischer, S.; Gao, J.; Guo, H.; Ha, S.; Joseph-McCarthy, D.; Kuchnir, L.; Kuczera, K.; T. K. Lau, F.; Mattos, C.; Michnick, S.; Ngo, T.; T. Nguyen, D.; Prodhom, B.; E. Reiher, W.; Roux, B.; Schlenkrich, M.; C. Smith, J.; Stote, R.; Straub, J.; Watanabe, M.; Wiórkiewicz-Kuczera, J.; Yin, D.; Karplus, M. All-Atom Empirical Potential for Molecular Modeling and Dynamics Studies of Proteins. *J. Phys. Chem. B* **1998**, *102* (18), 3586–3616 DOI: 10.1021/jp973084f.

(18) Mayne, C. G.; Saam, J.; Schulten, K.; Tajkhorshid, E.; Gumbart, J. C. Rapid Parameterization of Small Molecules Using the Force Field Toolkit. *J. Comput. Chem.* **2013**, *34* (32), 2757–2770 DOI: 10.1002/jcc.23422.

(19) Humphrey, W.; Dalke, A.; Schulten, K. VMD: Visual Molecular Dynamics. *J. Mol. Graph.* **1996**, *14* (1), 33–38 DOI: 10.1016/0263-7855(96)00018-5.

(20) Frisch, M. J.; Trucks, G. W.; Schlegel, H. B.; Scuseria, G. E.; Robb, M. A.; Cheeseman, J. R.; Scalmani, G.; Barone, V.; Petersson, G. A.; Nakatsuji, H.; Li, X.; Caricato, M.; Marenich, A.; Bloino, J.; Janesko, B. G.; Gomperts, R.; Mennucci, B.; Hratchian, H. P.; Ort, J. V.; Fox, D. J. Gaussian 09, Revision E.01. Gaussian, Inc.: Wallingford CT 2013.

(21) Marcus, Y. A Simple Empirical Model Describing the Thermodynamics of Hydration of Ions of Widely Varying Charges, Sizes, and Shapes. *Biophys. Chem.* **1994**, *51* (2–3), 111–127 DOI: 10.1016/0301-4622(94)00051-4.

(22) Abraham, M. J.; Murtola, T.; Schulz, R.; Páll, S.; Smith, J. C.; Hess, B.; Lindahl, E. GROMACS: High Performance Molecular Simulations through Multi-Level Parallelism from Laptops to Supercomputers. *SoftwareX* **2015**, *1–2*, 19–25 DOI:

10.1016/J.SOFTX.2015.06.001.

(23) Foote, H. W.; Hunter, M. A. Equilibrium in the System Ammonia-Ammonium Thiocyanate. *J. Am. Chem. Soc.* **1920**, *42* (1), 69–78 DOI: 10.1021/ja01446a010.

(24) Bussi, G.; Donadio, D.; Parrinello, M. Canonical Sampling through Velocity Rescaling. *J. Chem. Phys.* **2007**, *126* (1), 014101 DOI: 10.1063/1.2408420.

(25) Berendsen, H. J. C.; Postma, J. P. M.; van Gunsteren, W. F.; DiNola, A.; Haak, J. R. Molecular Dynamics with Coupling to an External Bath. *J. Chem. Phys.* **1984**, *81* (8), 3684–3690 DOI: 10.1063/1.448118.

(26) Parrinello, M.; Rahman, A. Polymorphic Transitions in Single Crystals: A New Molecular Dynamics Method. *J. Appl. Phys.* **1981**, *52* (12), 7182–7190 DOI: 10.1063/1.328693.

(27) IIAR. *Ammonia Data Book: The Profile of a Sustainable Refrigerant Chapter Two Properties of Ammonia (by International Institute of Ammonia Refrigeration)*, 2nd Ed.; Alexandria, Virginia, 2008.

(28) Abraham, M. J.; Gready, J. E. Optimization of Parameters for Molecular Dynamics Simulation Using Smooth Particle-Mesh Ewald in GROMACS 4.5. *J. Comput. Chem.* **2011**, *32* (9), 2031–2040 DOI: 10.1002/jcc.21773.

(29) Hess*, B. P-LINCS: A Parallel Linear Constraint Solver for Molecular Simulation. **2007** DOI: 10.1021/CT700200B.

(30) Shen, T.; Langan, P.; French, A. D.; Johnson, G. P.; Gnanakaran, S. Conformational Flexibility of Soluble Cellulose Oligomers: Chain Length and Temperature Dependence. *J. Am. Chem. Soc.* **2009**, *131* (41), 14786–14794 DOI: 10.1021/ja9034158.

(31) Liu, S.-H.; Rawal, T. B.; Soliman, M.; Lee, B.; Maxwell, T.; Rajasekaran, P.; Mendis, H. C.; Labbé, N.; Santra, S.; Tetard, L.; Petridis, L. Antimicrobial Zn-Based "TSOL" for Citrus Greening Management: Insights from Spectroscopy and Molecular Simulation. *J. Agric. Food Chem.* **2019**, *67* (25), 6970–6977 DOI: 10.1021/acs.jafc.9b02466.

(32) Nishiyama, Y.; Langan, P.; Chanzy, H. Crystal Structure and Hydrogen-Bonding System in Cellulose Ib from Synchrotron X-Ray and Neutron Fiber Diffraction. *J. Am. Chem. Soc.* **2002**, *124* (31), 9074–9082 DOI: 10.1021/ja0257319.

(33) Yang, M.; Zhao, W.; Wang, S.; Yu, C.; Singh, S.; Simmons, B.; Cheng, G. Dimethyl Sulfoxide Assisted Dissolution of Cellulose in 1-Ethyl-3-Methylimidazoium Acetate: Small Angle Neutron Scattering and Rheological Studies. *Cellulose* **2019**, *26* (4), 2243–2253 DOI: 10.1007/s10570-018-2218-0.

(34) Kumar, R.; Mago, G.; Balan, V.; Wyman, C. E. Physical and Chemical Characterizations of Corn Stover and Poplar Solids Resulting from Leading Pretreatment Technologies. *Bioresour. Technol.* **2009**, *100* (17), 3948–3962.

(35) Van Loon, L. R.; Glaus, M. A. *Experimental and Theoretical Studies on Alkaline Degradation of Cellulose and Its Impact on the Sorption of Radionuclides*; Villigen and Würenlingen, 1998.

(36) Haas, D. W.; Hrutfiord, B. F.; Sarkanen, K. V. Kinetic Study on the Alkaline Degradation of Cotton Hydrocellulose. *J. Appl. Polym. Sci.* **1967**, *11* (4), 587–600 DOI: 10.1002/app.1967.070110408.

(37) Chundawat, S. P. S.; Vismeh, R.; Sharma, L.; Humpula, J.; Sousa, L.; Chambliss, C. K.; Jones, A. D.; Balan, V.; Dale, B. E. Multifaceted Characterization of Cell Wall Decomposition Products Formed during Ammonia Fiber Expansion (AFEX) and Dilute-Acid Based Pretreatments. *Biores Technol* **2010**, *101*, 8429–8438 DOI: 10.1016/j.biortech.2010.06.027.

(38) Degroot, A. W.; Carroll, F. I.; Cuculo, J. A. A 13C-NMR Spectral Study of Cellulose and Glucopyranose Dissolved in the NH3/NH4SCN Solvent System. *J. Polym. Sci. Part A Polym. Chem.* **1986**, *24* (4), 673–680 DOI: 10.1002/pola.1986.080240410.

(39) Hudson, S. M.; Cuculo, J. A.; Wadsworth, L. C. The Solubility of Cellulose in Liquid Ammonia/Ammonium Thiocyanate Solution: The Effect of Composition and Temperature on Dissolution and Solution Properties. *J. Polym. Sci. Polym. Chem. Ed.* **1983**, *21* (3), 651–670 DOI: 10.1002/pol.1983.170210302.

(40) Gericke, M.; Schlufter, K.; Liebert, T.; Heinze, T.; Budtova, T. Rheological Properties of Cellulose/Ionic Liquid Solutions: From Dilute to Concentrated States. *Biomacromolecules* **2009**, *10* (5), 1188–1194 DOI: 10.1021/bm801430x.